Journal of Materiomics 10 (2024) 253–268

Contents lists available at ScienceDirect

Journal of Materiomics

journal homepage: www.journals.elsevier.com/journal-of-materiomics/

Review paper

Surface and structure engineering of MXenes for rechargeable batteries beyond lithium

Zefu Huang [a, 1], Majid Farahmandjou [a, 1], Frederick Marlton [a], Xin Guo [a], Hong Gao [b, ***], Bing Sun [a, **], Guoxiu Wang [a, *]

[a] Centre for Clean Energy Technology, School of Mathematical and Physical Sciences, Faculty of Science, University of Technology Sydney, Ultimo, NSW, 2007, Australia
[b] Joint International Laboratory on Environmental and Energy Frontier Materials, School of Environmental and Chemical Engineering Shanghai University, Shanghai, 200444, China

ARTICLE INFO

Article history:
Received 1 August 2023
Received in revised form
27 September 2023
Accepted 8 October 2023
Available online 29 October 2023

Keywords:
MXenes
Energy storage materials
2D materials
Surface engineering
Structure engineering

ABSTRACT

With the rapid growth in renewable energy, researchers worldwide are trying to expand energy storage technologies. The development of beyond-lithium battery technologies has accelerated in recent years, amid concerns regarding the sustainability of battery materials. However, the absence of suitable high-performance materials has hampered the development of the next-generation battery systems. MXenes, a family of 2D transition metal carbides and/or nitrides, have drawn significant attention recently for electrochemical energy storage, owing to their unique physical and chemical properties. The extraordinary electronic conductivity, compositional diversity, expandable crystal structure, superior hydrophilicity, and rich surface chemistries make MXenes promising materials for electrode and other components in rechargeable batteries. This report especially focuses on the recent MXene applications as novel electrode materials and functional separator modifiers in rechargeable batteries beyond lithium. In particular, we highlight the recent advances of surface and structure engineering strategies for improving the electrochemical performance of the MXene-based materials, including surface termination modifications, heteroatom doping strategies, surface coating, interlayer space changes, nanostructure engineering, and heterostructures and secondary materials engineering. Finally, perspectives for building future sustainable rechargeable batteries with MXenes and MXene-based composite materials are presented based upon material design and a fundamental understanding of the reaction mechanisms.

Contents

* Corresponding author.
** Corresponding author.
*** Corresponding author.
E-mail addresses: hgao1122@shu.edu.cn (H. Gao), bing.sun@uts.edu.au (B. Sun), guoxiu.wang@uts.edu.au (G. Wang).
Peer review under responsibility of The Chinese Ceramic Society.
[1] Zefu Huang and Majid Farahmandjou contributed equally to this work.

https://doi.org/10.1016/j.jmat.2023.10.001

1. Introduction

Renewable energy, generated from wind, solar, or tidal waves, has become an increasingly vital source of electricity generation over fossil fuels, when considering global sustainability, environmental conservation and climate change. As these renewable sources are intermittent, energy storage devices are required to ensure an uninterrupted and reliable energy supply. Due to the high energy conversion efficiency, relatively long lifespan, diverse range of energy and power densities, and cheap maintenance cost, rechargeable batteries are widely used for portable electronic devices, electric vehicles and grid energy storage. Lithium-ion (Li-ion) batteries have gradually dominated the energy storage market since their commercialization by SONY in 1991 [1]. However, the soaring prices of lithium due to the limited abundance in nature (*e.g.*, 0.002% in the earth's crust) make them less competitive for grid-scale adoption [2,3]. As a result, numerous novel rechargeable battery systems, also known as beyond-lithium batteries, that rely on more abundant elements, such as sodium (2.3%), potassium (2.1%), magnesium (2.3%), aluminum (8.2%) and zinc (0.0075%), have been explored and are showing substantial development. Importantly, among these elements, sodium and potassium have similar chemical properties to lithium because they all belong to the IA element group, and hence, have attracted more attention for the next-generation batteries. However, the large atomic radii of these ions leads to slow diffusion kinetics and considerable volume changes of the electrode materials during the charge and discharge processes, which significantly impacts the electrochemical performance of the batteries [4,5].

Current research activities regarding the appropriate cathode materials for these batteries are mainly focused on host materials with a framework structure that can accommodate the large transfer ions and provide competitive ionic and/or electronic conductivities, including olivine $FePO_4$ [6], Prussian blue analogue [7], and layered transition metals oxides (TMOs) [8]. By contrast, the development of anode materials is limited to carbon-based materials and metal compounds that can form alloys with alkali metal [9–13]. Among these electrode components, 2D materials such as transition metal dichalcogenides (TMDs), graphene, and TMOs show potential due to their unique and tunable morphologies [14–16]. Since 2012, a class of 2D transition metal carbide and nitride, known as MXene, has attracted attention. MXenes are derived by the selective exfoliation of 'A' layers with chemical etching from MAX phases [17–20] and share a general formula of $M_{n+1}X_nT_x$ (where M is an early transition metal, X is C or N, n is 1–4, and T_x stands for the terminated groups, such as –OH, –O, –F, *etc.*) [21]. They possess various physical and chemical properties, such as high hydrophilicity (*e.g.*, contact angle ≈ 21.5°–35.0°) [22], good mechanical properties, tunable interlayer distance and superior conductivity (*e.g.*, ≈ 9,880 S/cm for $Ti_3C_2T_x$, (3,250 ± 100) S/cm for V_2CT_x) [23]. These properties are beneficial for the development of advanced beyond-lithium batteries by increasing the electronic conductivity of the electrode materials, promoting the diffusion kinetics of large size ions in the electrode material, relieving the volume change of the electrode materials, guiding uniform platting and stripping of the transfer ions to suppress the dendrite growth, and retarding the "shuttle effect" of soluble species [24–28].

However, pristine MXenes show some drawbacks as anode materials for large ion storage, which restricts the development of high-performance beyond-lithium batteries in practical applications. This includes low specific capacity due to insufficient interlayer space to accommodate the transfer ions, and poor capacity retention due to the unreactive microstructure and undesirable surface functional groups. Therefore, many novel types of MXenes were developed to modify or enhance the surface and structure. This was achieved through advanced synthesis strategies, novel nanostructure engineering, regulating chemical composition, or integrating MXene with other premium electrode materials to form nanocomposites [19,29]. A critical summary of the recent progress in this area is desired to promote the development and applications of MXenes and MXene-based composites for next-generation batteries beyond lithium. Herein, we comprehensively review the advances of MXenes, focusing on their inherent merits for electrochemical devices, and the surface and structure engineering tactics for improving their performance in the batteries beyond lithium. Lastly, we conclude the current challenges in the area and propose several research directions for developing high-performance MXene-based electrode materials for building high-performance, sustainable, and economically viable batteries.

2. Structure and properties of MXene

As MXenes are primarily obtained from the layered MAX precursors (designated by $M_{n+1}AX_n$), it is essential to understand their crystal structure [30]. MAX phases are metallic and combine strong covalent M–X bonds with relatively weak M–A bonds [31]. The MAX phases belong to space group $P6_3/mmc$ and are comprised of a layered hexagonal structure. The 'A' element layers (mainly from groups of III-A or IV-A elements) are inserted between the closely packed 'M' layers (including Sc, Ti, V, Cr, Mn, Y, Zr, Nb, Mo, Hf, Ta, W and unlimited kinds of solid solution of these elements), which have octahedral sites occupied by the 'X' element atoms (C, and/or N). MXenes can be obtained by etching the 'A' group layers out from the MAX phases with HF, –F containing solutions or Lewis acid etchants. During this top-down synthetic process, surface terminations of 'T', depending on the reaction environment, are bonded to the M layers. The possible M, A, X, and T elements in MAX and MXene phases has been summarized in Fig. 1a. The MAX phases with different stoichiometries ($n = 1, 2, 3$) cause the ordering of M atoms to change from M_2X to M_3X_2 and M_4X_3 (Fig. 1b–c). For the M_2X structure, M atoms have a hexagonal close-packed stacking, while for M_3X_2 and M_4X_3 structures, M atoms follow a face-centered cubic stacking [31–33].

MXenes have unique and remarkable properties such as a low

electron transportation energy barrier, fast ion diffusion pathways, large specific surface area, functionalized surfaces, high electrochemical activity, and a high Young's modulus, which is due to their crystalline nature and ultra-thin layered structure. These properties result in high electronic and thermal conductivity, good hydrophilicity that enables easy combination with various species, superior physicochemical properties, and excellent flexibility. This makes MXenes very attractive for energy storage applications [34,35]. The specific physical and chemical properties of MXenes vary with different compositions and surface terminations. Currently, there are more than 100 stoichiometric MXene compositions that have been theoretically predicted, and over 30 of them have been experimentally prepared, enabling tuning their properties for a broad range of applications [29]. The detailed synthesis strategies and structure-property (*e.g.*, mechanical, electronic and chemical properties) relationships of MXenes, directly relating to their electrochemical energy storage performance, can be found in previous reports [36–41].

3. Advances and limitations of pristine MXenes for rechargeable batteries

Pristine MXenes here refer to MXenes that have been etched and exfoliated from the corresponding MAX phases without any further treatment to modify the surface or structure of the nanosheets. This section attempts to chronologically document some of the notable studies conducted on pristine MXenes for rechargeable batteries beyond lithium.

Lukatskaya et al. first demonstrated that a variety of cations, including, Na^+, K^+, NH_4^+, Mg^{2+}, and Al^{3+}, could be spontaneously intercalated into Ti_3C_2 MXene layers [42]. Their work partially instigated research into MXenes as promising electrode materials for alkali metal-ion batteries. Other early investigations involved screening MXenes as potential electrode materials using theoretical or computational methods. For example, using first-principles Density Functional Theory (DFT) calculations to investigate the adsorption energies of Li, Na, K and Ca atoms on Ti_3C_2. Er *et al.* unraveled the different relationships between adsorption energies and maximum coverage of alkali ions on MXenes, owing to their different ionic radii [5]. The adsorption energies of Li showed less sensitivity as the adatom coverage increased compared with Na, K and Ca counterparts. The theoretical specific capacities of MXenes for Li, Na, K, and Ca ion storage have been calculated to be 447.8, 351.8, 191.8 mA·h/g and 319.8 mA·h/g, respectively. Furthermore, they determined that due to the effective ionic radius of K, only about 60% adatom coverage on Ti_3C_2 monolayer was theoretically achievable. Moreover, they used the Nudged Elastic Band (NEB) method to investigate alkali-ion diffusion barriers on Ti_3C_2 MXenes, and reported values of 0.068, 0.096 eV and 0.103 eV for Li, Na, and K ions, respectively (Fig. 2a). These unique characteristics of MXenes show many advantages that make them worthy of further study in alkali-ion batteries.

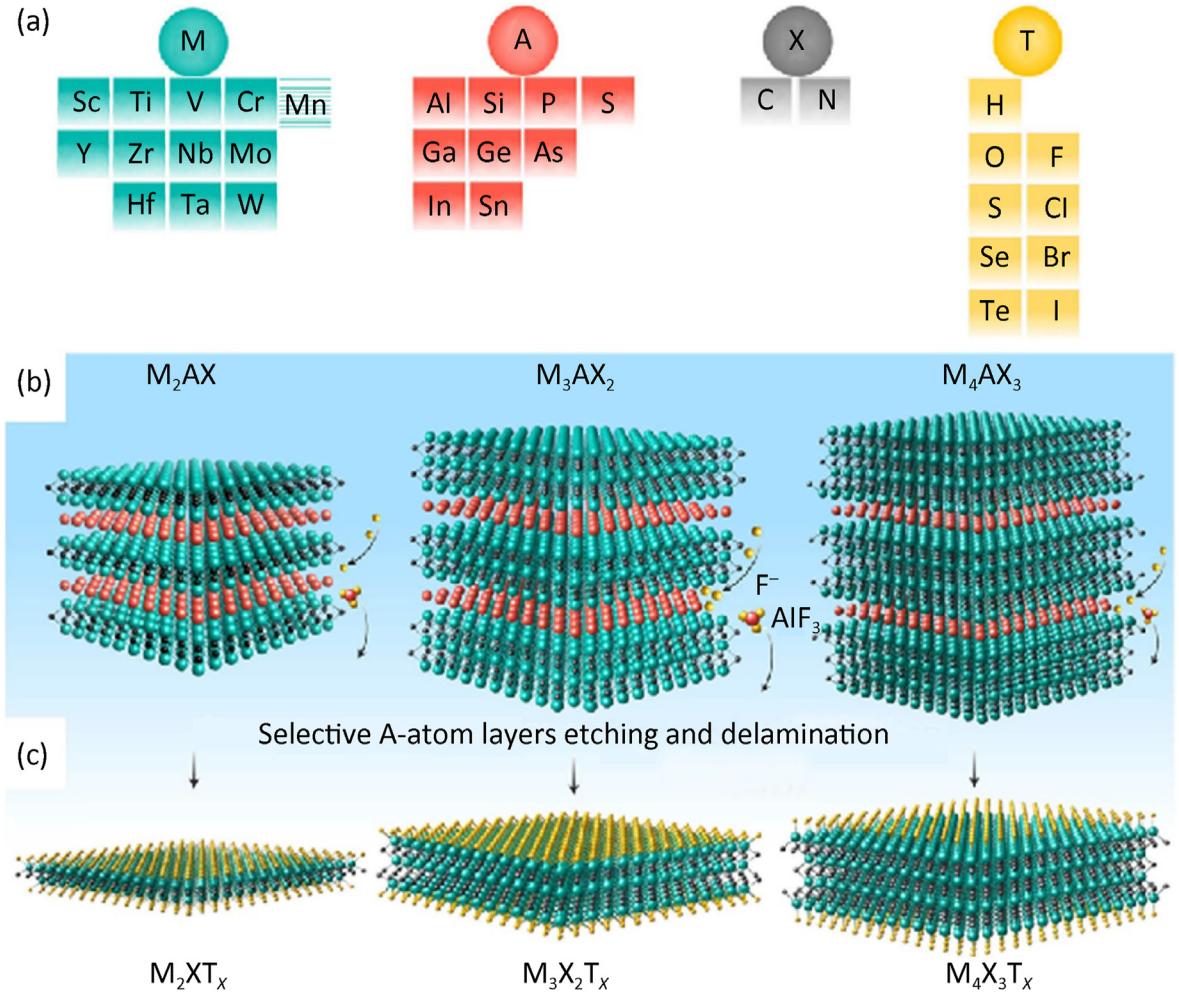

Fig. 1. (a) Possible elements of M, A, X, and T in MAX and MXene phases. (b) Schematic of MAX phases with M_2AX, M_3AX_2 and M_4AX_3 crystal structures. Layers of A group denoted by red atoms will be removed *via* an etching process. (c) Schematic of the obtained MXenes after the etching process. Formed surface terminations (labeled as 'T') are denoted by yellow atoms. Reproduced with permission [33]. Copyright 2020, Springer Nature.

Xie *et al.* theoretically disclosed that pristine (oxygen-terminated) MXenes had the lowest diffusion barriers when applied as electrode materials in non-Li-ion batteries, based on the $M_{n+1}C_nO_2A_2$ stoichiometry (where A is the alkali metal) (Fig. 2b) [43]. They confirmed their findings with a simple experiment involving terminated Ti_3C_2 MXene nanosheets. The charge storage mechanisms of MXenes were experimentally investigated in rechargeable batteries. When $Ti_3C_2T_x$ was implemented as an anode material in Na-ion batteries, it exhibited a reversible Na-ion intercalation mechanism (Fig. 2c) [44]. After the initial sodiation process, the interlayer space was demonstrated to remain stable and constant. This can be explained by the permanent intercalation of Na^+, which causes a 'pillaring' effect in the interlayer space (Fig. 2d), along with un-coordinated solvent molecules swelling the interlayer space. This pillaring effect serves to provide additional structural stability to the layered structure of MXenes, thereby allowing rapid Na-ion diffusion and good cycling stability. A similar Na intercalation mechanism was demonstrated for V_2CT_x MXene [45]. The study showed that the 'pillaring' effect caused by trapped Na^+ and un-coordinated solvent molecules within the interlayer space after the first sodiation/de-sodiation process was also evident for V_2C MXenes monolayers.

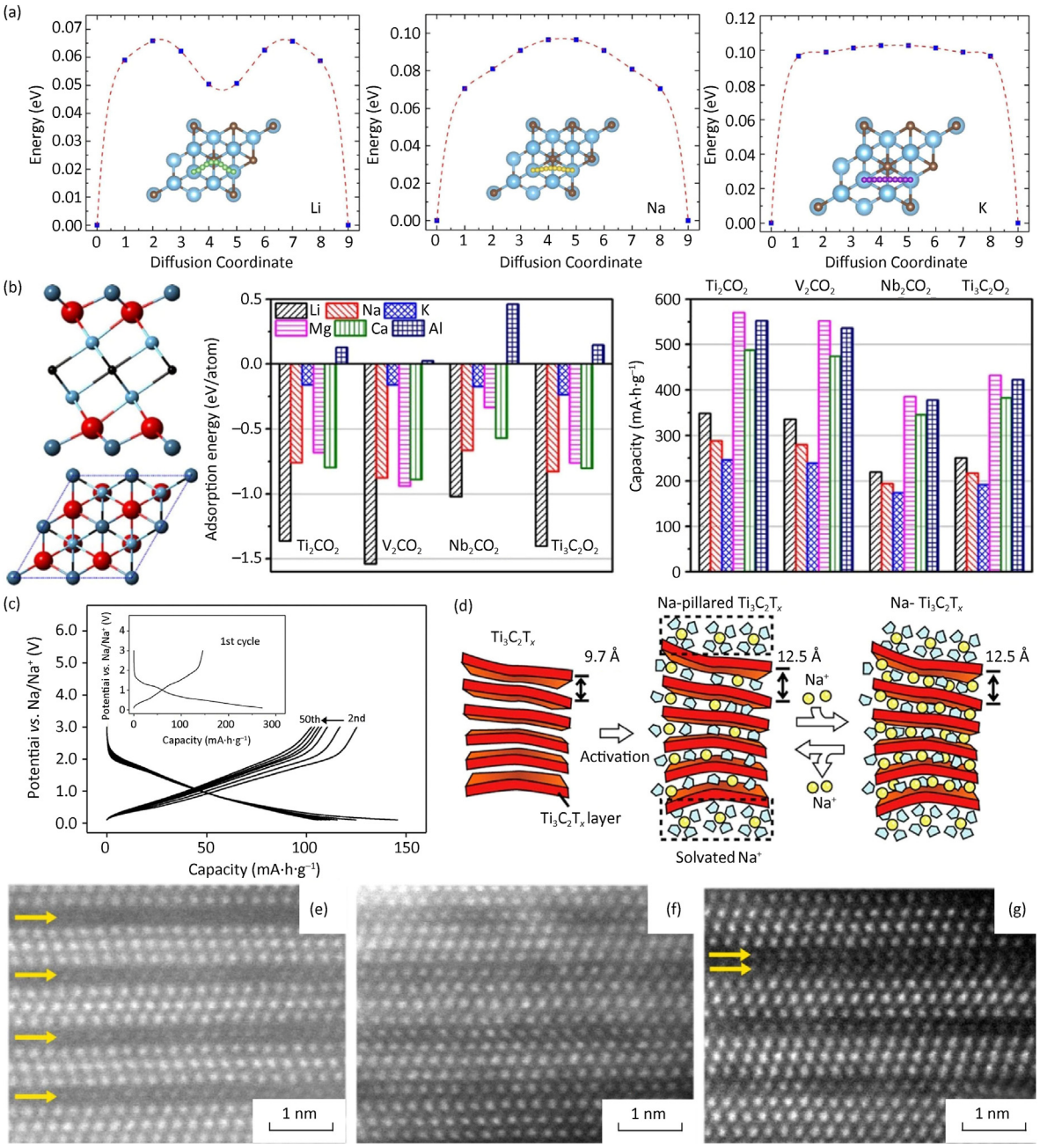

Fig. 2. (a) Schematic representation of the top view of the energetically optimized migration pathways and the corresponding diffusion barrier profiles of Li, Na, and K on Ti_3C_2 MXene. Reproduced with permission [5]. Copyright 2014, American Chemical Society. (b) Side and top views of ion adsorption on Ti_2CO_2 nanosheet, ion adsorption energies, and theoretical capacities on O-terminated MXene nanosheets. Reproduced with permission [43]. Copyright 2014, American Chemical Society. (c) Charge/discharge voltage profiles of $Ti_3C_2T_x$ MXenes in the first 50 cycles at 20 mA/g. (d) Schematic of Na^+ insertion mechanism into $Ti_3C_2T_x$. Reproduced with permission [44]. Copyright 2016, American Chemical Society. (e–g) The high-angle annular dark-field (HAADF) images of Ti_3C_2X electrodes upon Na^+ intercalation. Na^+ are (e) partially or (f–g) fully intercalated into Ti_3C_2X from the surface. Two layers of sodium can be seen intercalated into one interlayer, indicated by yellow arrows in (g). Reproduced with permission [46]. Copyright 2015, American Chemical Society.

Wang *et al.* reinforced the understanding of Na^+ intercalation mechanisms for $Ti_3C_2T_x$ monolayers, demonstrating that Na^+ are intercalated near the surface of MXenes before being diffused into the bulk [46]. Upon extended sodiation, double layers of Na^+ could be inserted into the same interlayer space, which indicated that increasing interlayer space could be a promising route to improve the capacity of MXene materials in Na-ion batteries (Fig. 2e–g). They also used experiment to demonstrate that in the stacked MXene interlayers, Na^+ preferred to stay on top of the carbon atoms, thus shifting the surface terminal group towards the central Ti which stabilized the macrostructure. Their extensive study provided important insight into Na^+ intercalation mechanisms of MXenes. First-principles swarm structure calculations were conducted by Yu et al. to compute the theoretical specific capacity of 2D single atomic layer of TiC_3 for sodium storage, which is as high as 1,278 mA·h/g and approximately three times the theoretical capacity of metal-rich MXenes, such as Ti_3C_2 and Ti_2C (370 mA·h/g and 359 mA·h/g, respectively) [47]. It attests that increasing the carbon content in the matrix stoichiometry and controlling the thickness of MXene improves the electrochemical performance as an anode material in Na-ion batteries.

When Ti_3CNT_x was experimentally investigated as an anode material for K-ion batteries, it was shown that K^+ also had the 'pillaring' effect, where K-ions were trapped in the interlayer space. This could be caused by the reactions of K^+ with the MXene surface terminal groups, or by the trapped solvent and/or residual etching products [48]. This is evidenced by a largely irreversible capacity loss and a permanent increase of the interlayer space after the first cycle. This study indicates that Ti_3CNT_x might be a promising anode material for K-ion batteries if the irreversible capacity loss after the first cycle can be mitigated. V_3C_2 MXene monolayers were also theoretically proven to be a potential anode material for Li, Na, K and Ca batteries [49]. They found that the theoretical capacities of V_3C_2 are 606.42 mA·h/g for both Li and Na, 269.86 mA·h/g for K, and 539.71 mA·h/g for Ca. They also used Nudged Elastic Band (NEB) method to obtain diffusion barriers with the values of 0.04, 0.02, 0.01 eV and 0.04 eV for Li, Na, K and Ca, respectively.

Pristine MXenes have generally tended to be inefficient electrode materials for alkali metal-ion batteries. Even after exfoliation or delamination to a single or a few layers, the 2D nanoflakes show a tendency to restack into multiple-layers and agglomerate during the electrode preparation process, reducing the available intercalation sites and resulting in low capacity and poor cycling performance.

4. Methodology of surface and structure engineering for MXenes

Most of the electrochemical reactions regarding MXenes in battery systems are concerned with the surface function and the structural morphology. The surface engineering, by modifying the terminal surface group T_x, is the most straightforward method to change the surface function of MXene (Fig. 3a). Common T_x groups are −F, −O and −OH, where the −F terminations are beneficial in the establishment of stable solid electrolyte interphase (SEI) during electrochemical reactions, and −O and −OH groups provide a more stable thermodynamic performance in batteries [50,51]. Other types of T_x terminations, such as −Cl and −Br, obtained by using the novel molten Lewis acidic salt etching method, could be very helpful to extend the surface modification and application of MXene in the future [52]. Other surface engineering strategies, such as heteroatom doping including non-metal and metal cooperation (Fig. 3b) and surface coating strategy (Fig. 3c), are also widely researched and applied to offer enhanced electrochemical performance of the MXene in the beyond-lithium batteries [53,54]. The modification of the structure is another promising path to alter MXene electrochemical characters in battery systems. As the radius of transfer ions are generally larger in the battery systems beyond-lithium than the conventional Li–based batteries, the structural engineering becomes very important for battery design. The most direct strategy is to increase the interlayer distance of MXene (Fig. 3d). By introducing large ions like Sn^{2+} and cetyltrimethylammonium cation (CTA^+) as the pillars between the adjacent MXene layers, the electrode can fulfil the ion transport requirement for large-size ions like Na^+ or K^+ [55–57]. Additionally, changing the 2D layer-like structure in MXenes can offer high electrochemical performance in the beyond-lithium batteries. This can be achieved through nanostructure engineering (Fig. 3e), heterostructure engineering, or introducing secondary materials in the 3D framework with various structural morphologies (Fig. 3f) [22,58–62]. A development timeline of surface and structure engineering strategies supported by some representative works is shown in Fig. 3g, where we can see the research initiated from the interlayer spacing engineering, surface termination modifications to architecture construction and composites fabrication. Many recent works on developing MXene-based electrode materials for rechargeable batteries beyond lithium synergizing two or more of these strategies to achieve boosted performances.

5. Surface-engineered MXenes for rechargeable batteries beyond lithium

5.1. Surface terminations engineering

The different types of surface terminations on MXenes directly influence their charge storage performance. The −F, −O, −OH or −Cl terminations have a distinct molecular mass, leading to different theoretical capacities, even based on the same intercalation mechanism. Moreover, the functional groups on MXenes also influence the reaction kinetics and thereby result in diverse electrochemical performance. Xie *et al.* firstly indicated the O-terminated and bare MXenes can be promising anode material for batteries beyond lithium [43]. Recently, Chen *et al.* carried out first-principal calculations to characterize two proposed sulfurized MXenes, Ti_2CS_2 and Ti_2NS, as potential anode materials for K-ion batteries [64]. Their study indicates that the K adatom possesses low adsorption energies of −2.72 eV and −2.37 eV and that the diffusion energy barriers are 0.046 eV and 0.048 eV for Ti_2CS_2 and Ti_2NS_2, respectively. These MXenes are predicted to allow a complete adsorption layer and rapid kinetics for both surfaces of one single layer MXene. These factors contribute towards a high theoretical specific capacity of the 390 mA·h/g and 381 mA·h/g (assuming bilayer adsorption) for Ti_2CS_2 and Ti_2NS_2, respectively.

Bao *et al.* successfully prepared a wrinkled S-doped MXene ($S–Ti_3C_2T_x$) as the sulfur cathode hosts for room temperature sodium-sulfur (RT Na–S) batteries (Fig. 4a) [53]. The as-prepared S-doped MXene hosts offered a high sulfur loading of up to 4.5 mg/cm^2 due to its large specific surface area and porous structure (Fig. 4b–c). They also improved the electronic conductivity of the sulfur cathodes and provided strong chemical confinement to restrict the shuttling of soluble Na polysulfides due to their high polarity functional groups. Thus, the S-doped MXene host cathode delivered a high initial capacity of around 822 mA·h/g and remained a reversible capacity of 577 mA·h/g after 500 cycles at a current rate of 2 C.

Natu *et al.* reported a method to synthesize MXenes without using water as the solvent, which resulted in F-rich terminations [65]. They utilized the polar organic solvents containing NH_4HF_2, where the NH_4HF_2 will dissociate into NH_4F and HF in the polar solvents. Therefore, the HF in the organic solvent plays the same

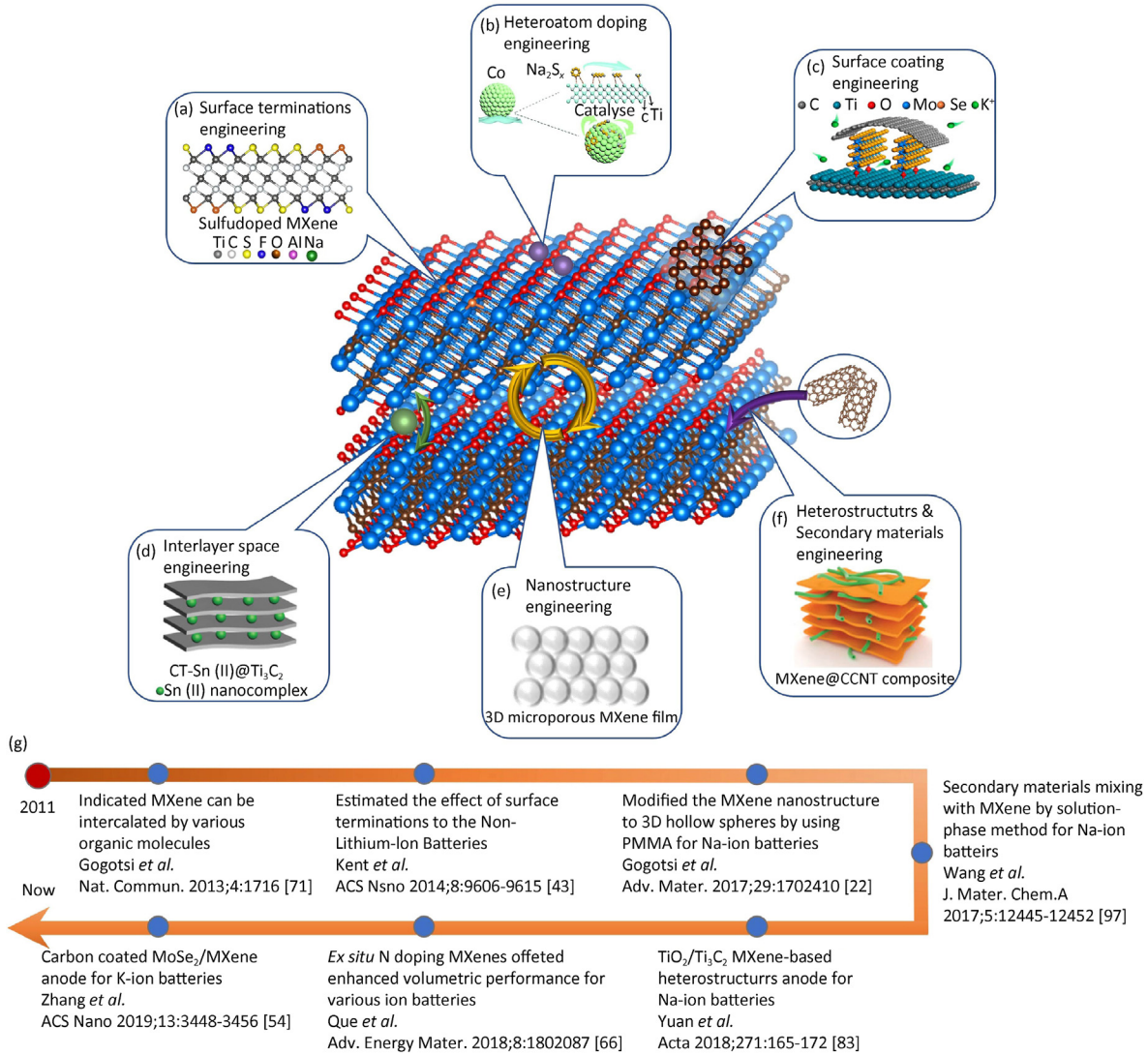

Fig. 3. Summary and development timeline of the surface and structure engineering for MXene application in rechargeable batteries beyond lithium. Surface engineering: (a) Surface terminations engineering. Reproduced with permission [53]. Copyright 2019, American Chemical Society. (b) Heteroatom doping engineering. Reproduced with permission [63]. Copyright 2020, Royal Society of Chemistry. (c) Surface coating engineering. Reproduced with permission [54]. Copyright 2019, American Chemical Society. Structure engineering: (d) Interlayer space engineering. Reproduced with permission [55]. Copyright 2018, WILEY-VCH. (e) Nanostructure engineering. Reproduced with permission [22]. Copyright 2017, WILEY-VCH. (f) Heterostructures and secondary materials engineering. Reproduced with permission [60]. Copyright 2020, WILEY-VCH. (g) The development timeline of the strategies indicated by some representative works.

role as in water for the etching process. The as-prepared F-rich terminated $Ti_3C_2T_x$ was tested as the anode material in Na-ion batteries with carbonate electrolytes, and it offered approximately double the capacity compared to an MXene obtained by etching in water with O-rich terminates.

5.2. Heteroatom doping

Heteroatom doping, including non-metallic and metallic atom doping, aims to provide more electrochemically active sites to improve ion transport kinetics, electronic conductivity, and the electrochemical reaction rate. Yang *et al.* modified the $Ti_3C_2T_x$ surface with nitrogen (N) doping that significantly enhanced the material's volumetric capacitance, which illustrates promising potential for various applications in ion storage [66]. Zhang et al. synthesized the $Mo_2TiC_2O_2$-Pt_{SA} by doping the Pt to occupy the Mo vacancies which effectively improved the charge transfer and conversion reaction kinetics [67].

Heteroatom doping can also cooperate with structural modification to catalyze the conversion reactions in metal-sulfur/air batteries [68]. For example, Wang *et al.* doped Co with boron-carbon-nitrogen nanotubes (BCN) onto TiCN to form the cathode TiCN–BCN–Co for Zn-air batteries. The TiCN–BCN–Co cathode they designed provided an excellent oxygen reduction reaction (ORR) activity with better stability and tolerance to methanol than commercial Pt/C. As a result, their batteries with TiCN–BCN–Co cathode offered a high specific capacity of 791 mA·h/g with 200 h of stable cycling [69]. Yang et al. reported a Co-doped MXene-based hybrid 3D porous host of $Ti_3C_2T_x$/rGO with cobalt nanoparticles (MG-Co) for sulfur cathodes (Fig. 4d–e) [63]. The cobalt nanoparticles with catalytic characteristics provided strong chemical adsorption and accelerated conversion of the soluble long-chain Na polysulfides to insoluble short-chain Na polysulfides, which effectively suppressed the shuttle effect. Thereby, the RT Na–S battery with MG-Co cathode delivered a high average capacity of 705 mA·h/g at 0.1 C and good cycling performance with a reversible capacity of 360 mA·h/g after 200 cycles at 0.5 C.

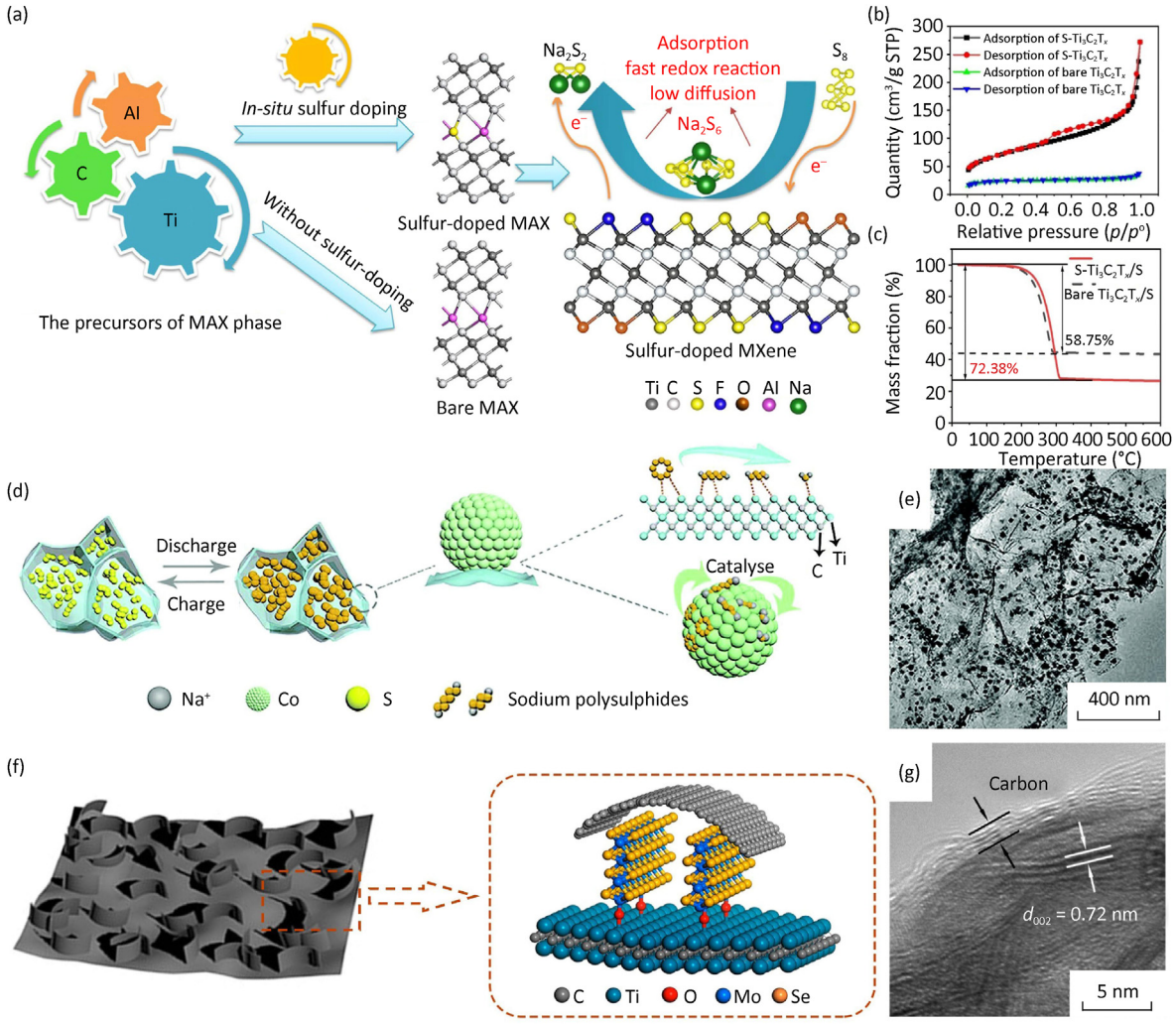

Fig. 4. (a) Schematic of doping S into the MXene layer and the chemical adsorption mechanism of MXene to sodium polysulfides. (b) Specific surface area of S–$Ti_3C_2T_x$ and bare $Ti_3C_2T_x$ samples showing by the nitrogen adsorption-desorption curve. (c) Sulfur loading of the S–$Ti_3C_2T_x$/S composite showing by TGA curve. Reproduced with permission [53]. Copyright 2019, American Chemical Society. (d) Schematic of the catalytic effect of cobalt nanoparticles and (e) TEM image of the MXene attached with Co nanoparticles. Reproduced with permission [63]. Copyright 2020, Royal Society of Chemistry. (f) Schematic of the $MoSe_2$/MXene nanosheets coated with carbon. (g) HRTEM image of the carbon coated $MoSe_2$/MXene material. Reproduced with permission [54]. Copyright 2019, American Chemical Society.

5.3. Surface coating

Another type of surface engineering strategy, surface coating, can improve the chemical and structural stability as well as the electronic and ion conductivity of MXene-based electrodes. Carbonaceous materials are commonly applied as coatings on the MXene nanosheets due to their excellent conductivity, high electrochemical stability, low cost, and accessibility.

For instance, Huang *et al.* designed the $MoSe_2$/MXene hybrid nanosheets coated with carbon to form the $MoSe_2$/MXene@C anode for K-ion batteries (Fig. 4f–g) [54]. The carbon coating strategy effectively enhanced the electronic conductivity and maintained the morphology of the MXene-based anode and thus enhanced the specific capacity, cycling stability, and rate capability. Consequently, the K-ion batteries with the $MoSe_2$/MXene@C anode offered a high capacity retention of 355 mA·h/g after 100 cycles at 200 mA/g. More recently, Zhang et al. reported a hierarchical porous N-doped carbon (HPNC) coated fluorine-free $Ti_3C_2T_x$ cathode by using a one-pot etching synthesis strategy [70]. The HPNC coating layers successfully modify the MXene surface which offers a higher binding energy, reduces the energy barriers, and thus, improves the confinement of soluble polysulfides and the redox kinetics. This design demonstrates a novel synthesis method to exploit surface coating engineering for improving the electrochemical performance of MXene-based materials at room temperature with a S/Se-based cathode.

Overall, owing to their rich surface chemistries and highly tunable characters, MXenes have numerous surface engineering strategies and huge potential to build up the conductive frameworks for improving the electrochemical performance of beyond-lithium batteries by maintaining the high electronic conductivity, alleviating volume change, and providing homogeneous ion transport flux.

6. Structure-engineered MXenes for rechargeable batteries beyond lithium

6.1. Interlayer space engineering

The tunable interlayer space of MXenes makes them attractive for energy storage applications, particularly as intercalation-type electrode materials. It can be easily realized by using a variety of intercalant species, such as organic molecules and cations. Mashtalir *et al.* found that intercalating hydrazine together with N,N-

dimethylformamide molecules greatly increased the c-lattice parameter of $Ti_3C_2T_x$ from 19.50 Å to 25.48 Å and then to 26.80 Å [71]. Reversible humidity-dependent expansion of the $Ti_3C_2T_x$ MXenes intercalated with cations (*e.g.*, Li^+, Na^+, K^+, Rb^+, Mg^{2+} or Ca^{2+}) was also observed [72], and the interlayer space range increased from 12.50 Å to 15.5 Å. Wu et al. synthesized few-layered $Ti_3C_2T_x$ by intercalating the multilayered MXene with dimethyl sulfoxide (DMSO) and then subjecting the material to high energy ball milling to yield f-$Ti_3C_2T_x$_DMSO [73]. The f-$Ti_3C_2T_x$_DMSO electrode applied in the Na-ion batteries as anode demonstrated a reversible capacity of 267 mA·h/g at 100 mA/g, and a stable capacity of 196 mA·h/g was maintained after 500 cycles. Moreover, a capacity of 110 mA·h/g can be achieved at a super high current density of 2 A/g.

Luo *et al*. made a notable attempt to modify the interlayer space of MXenes through intercalation of the Sn^{2+} (Fig. 5a–b) [55]. In their initial study, they synthesized a Sn^{2+} pillared Ti_3C_2 MXene matrix by pre-intercalating the pristine MXene with cetyltrimethylammonium bromide (CTAB) to obtain a stable 'pillared' structure and then intercalated the Sn^{2+} by ion-exchange with the CTA^+. Based on this work, they used a similar idea to intercalate sulfur into the Ti_3C_2 interlayer space, thus synthesizing the S intercalated Ti_3C_2 (CT-S@Ti_3C_2) [74]. The pristine MXene was pretreated with CTAB, followed by heat diffusion of elemental S, and ending with an annealing process at various high temperatures. The X-ray Photoelectron Spectroscopy (XPS) results indicated that the ratio of Ti–S bonds was the highest when annealed at 450 °C, corresponding to the best electrochemical performance of the as-prepared materials. The analysis, reinforced with theoretical calculations, confirmed that the excess S atoms provided enlarged interlayer space, which facilitated fast diffusion kinetics along with the S-functionalized interlayer. When tested in half cells with the sodium anodes, the as-prepared materials demonstrated impressive Na-ion storage capability and rate performance with discharge capacities of 531 mA·h/g at 0.1 A/g and up to 120 mA·h/g at 15 A/g.

Luo *et al*. also discovered that the interlayer space of $Ti_3C_2T_x$ MXene is affected by cationic surfactants with different lengths of hydrophobic alkyl chains [56]. The pillared $Ti_3C_2T_x$ MXene with CTAB intercalation has an enlarged interlayer space of 2.708 nm, which is 177% greater than the pristine MXene (0.977 nm). Li et al. studied the effects of partial sulfur doping on the carbon sites of the Ti_3C_2 MXenes [57]. They doped sulfur into Ti_3C_2 by HF etching Ti_3AlC_2 and subsequent sulfidation using thiourea as the sulfur source. The large S atoms doped on some of the carbon sites in the Ti_3C_2 layers served to increase the interlayer space. Combing with the pillaring effect of trapped Na ions, the layered morphology shows remarkable stability. These factors combined with the pseudocapacitive nature observed in the Na-ion storage mechanism highlight the intriguing effects of sulfur doping.

Recently, Han's group successfully incorporated Sb ultrafine particles onto the few-layered MXene nanosheets (f-$Ti_3C_2T_x$) to form the Sb/p-$Ti_3C_2T_x$ as the anode for Na-ion batteries [75]. With the benefits from few-layered MXenes, pillaring technique, and strong chemical bonding of Ti–O–Sb, the Sb/p-$Ti_3C_2T_x$ anode exhibited an enhanced structural stability and conductivity. Consequently, the Na-ion batteries with Sb/p-$Ti_3C_2T_x$ anode offered a significantly improved cycling stability with 350.6 mA·h/g capacity retention after 100 cycles at 50 mA/g.

6.2. Nanostructure engineering

An alternative strategy to reduce layer stacking and enhancing the electrochemical performances of MXenes include using 2D nanosheets to construct 3D porous, crumpled, or hollow spherical structures. These strategies increase the active specific surface area for fast alkali ion transport and provide an abundant porous structure for electrolyte impregnation.

Zhao *et al*. reported that 2D MXene nanosheets can be converted into a 3D hollow sphere structure [22]. The 3D hollow spheres of $Ti_3C_2T_x$, V_2CT_x and Mo_2CT_x were synthesized by first mixing polymethyl acrylate (PMMA) spheres with the solutions containing the 2D delaminated nanosheets. During the mixing procedure, the MXene nanosheets covered the surfaces of PMMA spheres due to the interaction of the hydroxyl surface groups of MXenes with PMMA. The porosity of the final products can be fine-tuned by changing the size of the PMMA spheres. After vacuum filtration and annealing processes, the PMMA precursors can be removed and a flexible 3D porous film with promising properties can be obtained (Fig. 5c). The cross-sectional SEM images of the obtained 3D porous V_2CT_x and Mo_2CT_x films are shown in Fig. 5d and e, respectively. When the 3D porous $Ti_3C_2T_x$, V_2CT_x, and Mo_2CT_x films were directly used as the anodes in Na-ion batteries, they exhibited highly reversible capacities of approximately 295, 310 mA·h/g and 290 mA·h/g, respectively, at the current rate of 2.5 C. The pseudocapacitance dominated by Na-ion storage mechanism contributed to the stable cycling performance of up to 1,000 cycles at nearly 100% Coulombic efficiency.

Lian *et al*. alkalized and delaminated accordion-like multilayer MXenes (*i.e.*, HF-etched Ti_3C_2), by shaking/stirring them in KOH solution [77]. A combination of the shaking/stirring caused a series of reactions for the substitution of –F terminal groups with –OH groups, leading to a fast diffusion rate of K^+ into the interlayer space. This promoted the delamination of thin O-terminated MXene nanoribbons and self-assemble of a 3D porous structure. When tested as anodes in K/Na-ion batteries, the materials demonstrated fast reaction kinetics, enhanced reversible capacities, and improved cycling stability in comparison to the pristine MXenes. However, the performance of the 3D porous O-terminated MXenes at current densities above 200 mA/g is nearly identical to that of unmodified MXenes [77]. Similarly, ultrathin nanoribbons of sodium titanate ($NaTi_{1.5}O_{8.3}$, M-NTO) and potassium titanate ($K_2Ti_4O_9$, M-KTO) were also successfully fabricated through concurrent oxidation and alkalisation processes of pristine Ti_3C_2 MXenes [78].

Natu *et al*. demonstrated that 2D MXene nanosheets would crumple and 'crash out' or flocculate into mesoporous 3D powders by simply decreasing the pH value of the same colloidal suspension. The obtained materials exhibited promising electrochemical performances as anode materials in Na-ion batteries [79]. In another investigation, they proved that a similar crumpled mesoporous structure could be attained by increasing the pH value of a colloidal suspension of $Ti_3C_2T_x$ using common alkali metal hydroxides [80]. Xie et al. designed and constructed a porous anisotropic $Ti_3C_2T_x$ (p-$Ti_3C_2T_x$) macrostructure by using a sulfur-based template, which mitigated the restacking of MXene nanosheets and promoted high rate performance and long-term cycling stability [81]. The crumpled 2D sheets spontaneously arranged into a porous structure, which retained a high capacity of 189 mA·h/g after 1,000 cycles at the high current density of 1 A/g. This material potentially prevents the need to consider a trade-off between power and energy densities, because of the efficient ion storage mechanism, along with the ultra-fast diffusion kinetics, as revealed by cyclic voltammograms (CV) analysis.

Recently, Zhao *et al*. reported a K^+ pre-intercalated $Ti_3C_2T_x$ (K^+-$Ti_3C_2T_x$) with a porous framework and enlarged interlayer distance as a high-performance electrode material for K-ion hybrid capacitors (Fig. 5f–g) [76]. The 3D porous architecture was prepared through electrostatic flocculation followed by a subsequent freeze-

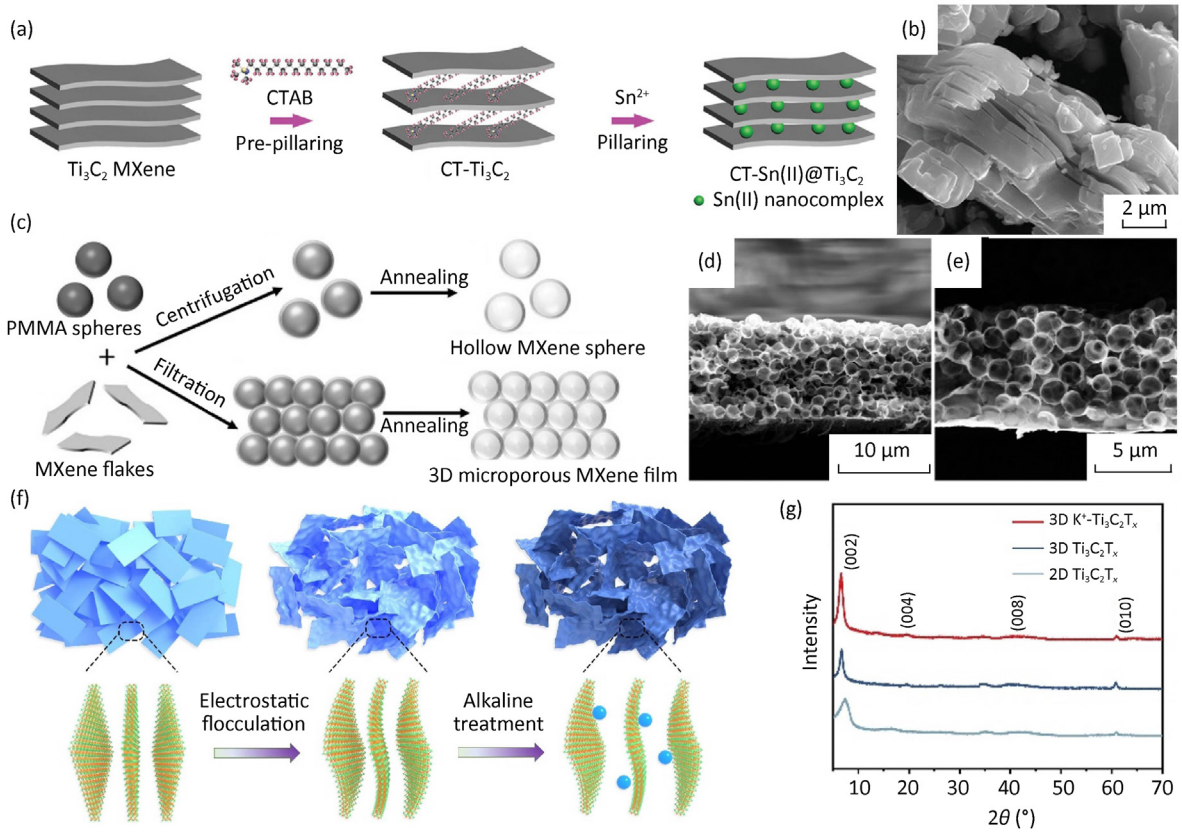

Fig. 5. (a) Schematic of inserting Sn^{2+} pillars into the interlayer space of MXene nanosheet. (b) SEM image of MXene with Sn^{2+} pillars. Reproduced with permission [55]. Copyright 2018, WILEY-VCH. (c) Schematic showing the synthesis of hollow MXene spheres and 3D macroporous MXene frameworks. Cross-sectional SEM image of the 3D macroporous (d) V_2CT_x and (e) Mo_2CT_x films. Reproduced with permission [22]. Copyright 2017, WILEY-VCH. (f) Schematic of the synthesis process of 3D K^+—$Ti_3C_2T_x$. (g) XRD patterns of the 3D K^+—$Ti_3C_2T_x$, 3D $Ti_3C_2T_x$, and 2D $Ti_3C_2T_x$. Reproduced with permission [76]. Copyright 2021, Wiley-VCH.

drying process. Subsequently, the 3D $Ti_3C_2T_x$ was treated in KOH solution to obtain the K^+ intercalated MXene with a larger interlayer distance of 1.32 nm. The unique structure of K^+-$Ti_3C_2T_x$ significantly reduces the structural distortions during the potassiation and depotassiation processes. Moreover, a thin and stable SEI was formed by modifying the concentration of ether-based electrolyte, consequently improving the overall performance of the as-prepared materials.

In conclusion, a variety of approaches have been used to optimize the interlayer space and nanostructure of MXenes. The modified MXenes with more accessible active sites and faster reaction kinetics showed remarkably enhanced electrochemical performance in comparison to the original MXenes. These studies boost the development of the MXene family for future energy storage applications.

6.3. Heterostructure engineering

Owing to their rich surface chemistries, MXenes can be used as the template to bond or grow various materials such as TiO_2 [82,83], SnO_2 [82], $NiCo_2Se_4$ [61], CuS [84], P [85], and $Na_3Ti_5O_{12}$ [62]. This is known as heterostructure engineering and fulfills the requirements of different electrodes for different batteries. In the heterostructure engineering process, the MXene template forms strong chemical bonds with the loading hetero materials, which results in the homogeneous distribution of dopants and improves the ion/electron transport inside the electrodes. The loading materials also act as spacers to prevent the restacking of MXene nanosheets and additional reservoirs to store active cations.

The construction of MXene-based heterostructures can be realized by oxidation, sulfurization, fluorination, chlorination, or nitridation of the MXene nanosheets. For example, Yang et al. reported an accordion-like TiO_2/Ti_3C_2 anode material derived from $Ti_3C_2T_x$ with surface oxidation to obtain TiO_2 components loaded on the nanosheets [83]. This strategy formed a homogeneous decoration of TiO_2 on the MXene surface, which enabled more efficient Na ion storage and ion diffusion. Consequently, the Na-ion batteries with TiO_2/Ti_3C_2 composite as anodes demonstrated a high reversible capacity of 101 mA·h/g after 500 cycles at 200 mA/g.

Utilizing the cations trapped by MXene nanosheets as seeds to *in situ* grow a new phase is another strategy to obtain heterostructures. Recently, Han's group used a one-step solvothermal process to design a $NiCo_2Se_4$/f-Ti_3C_2 (few-layered Ti_3C_2) electrode material with heterostructure (Fig. 6a–b), which exhibited good performance in Na-ion batteries [61]. During the formation, they used the electrostatic attracting method to dope the Ni^{2+} and Co^{2+} onto the f-Ti_3C_2 flakes. This was followed by the solvothermal process with selenium powder to form $NiCo_2Se_4$ loaded on the f-Ti_3C_2 surface. The strong Ti—O—Ni chemical bonds ensure the $NiCo_2Se_4$ nanoparticles distribute on the MXene flakes. The anchored $NiCo_2Se_4$ nanoparticles prevented the restacking of MXene nanosheets and improve the ion/electron diffusion. Consequently, Na-ion batteries with a $NiCo_2Se_4$/f-Ti_3C_2 anode provided superior cycling stability with 379.2 mA·h/g capacity that remained after 100 cycles at 100 mA/g. Similarly, they exploited residual Cu atoms within the MXene flakes that were synthesized by $CuCl_2$•$2H_2O$-based Lewis acidic etching method as seeds to *in situ* grow CuS on the $Ti_3C_2T_x$ nanosheets *via* a sulfurization

treatment (Fig. 6c). The as prepared electrode provided relatively lower adsorption energy to Na ($Ti_3C_2T_x$/CuS: −2.78 eV *vs.* CuS: −2.09 eV), increased interlayer space (Fig. 6d), and strong interfacial bonding, which improved Na-ion storage, ion/electron transport kinetics, and structural stability.

Moreover, the transition metal atoms (M) at the outer layer of $M_{n+1}X_nT_x$ can be used as seeds to *in situ* grow hetero materials on the surface of MXene. Luo et al. fabricated a $Na_3Ti_5O_{12}$-MXene hybrid framework by pre-treating the MXene (Ti_3C_2) with CTAB and then oxidized them in NaOH solution to grow the $Na_3Ti_5O_{12}$ nanowires on the MXene surface as pillars between the MXene layers [62]. The $Na_3Ti_5O_{12}$ nanowires supported the wide interlayer space, which offered stable and appropriate Na-ion diffusion channels. Meanwhile, the functional groups of MXenes guided the Na nucleation inside the porous scaffold. Thereby, the CTAB pre-treated MXene after 3 days of oxidation in NaOH solution (denoted as C-NTO-3) provided excellent Na adsorption capability and guided homogenous Na plating (Fig. 6e–f). In symmetric cell testing, the C-NTO-3/Na electrodes offered a much lower interfacial resistance (≈7 Ω) than that of Cu/Na electrodes (≈56 Ω) after 30 cycles, due to the formation of a stable SEI and uniform Na deposition. Moreover, the RT Na–S cells with C-NTO-3/Na anodes delivered improved Coulombic efficiencies and smaller voltage polarization than the cells with pristine Na anodes (Fig. 6g), which indicated the C-NTO-3/Na anodes could also improve the reaction kinetics and restrict polysulfide shuttling. Consequently, the RT Na–S cells with C-NTO-3/Na anodes provided a high reversible capacity of 456 mA·h/g after 500 cycles at a current density of 0.5 C.

6.4. Secondary materials engineering

Although great efforts have been made to improve the electrochemical performance of MXenes in rechargeable batteries, the achieved capacities of pure or heterostructure MXenes are still less competitive due to the low theoretical capacity based on the intercalation mechanism. Many potential strategies are being explored for the rapid synthesis and testing of new nanomaterials, as well as the incredible diversity of capabilities that may be achieved by combining different materials. To boost the capacities and energy densities of MXenes, researchers have utilized this strategy to produce MXene-integrated composites or hybrids that effectively exploit the electrochemical benefits of each individual nanomaterial [82].

6.4.1. MXene with carbon-based material

Carbon-based materials are ideal secondary materials when combined with MXene to achieve high performance owing to their high conductivity, structural diversity and low cost. Recently, 3D porous frameworks built up from MXene nanosheets combined with carbon-based materials have shown potential to fulfil the above requirements to boost the electrochemical performances of beyond-lithium alkali metal anodes. For instance, Tang *et al.*

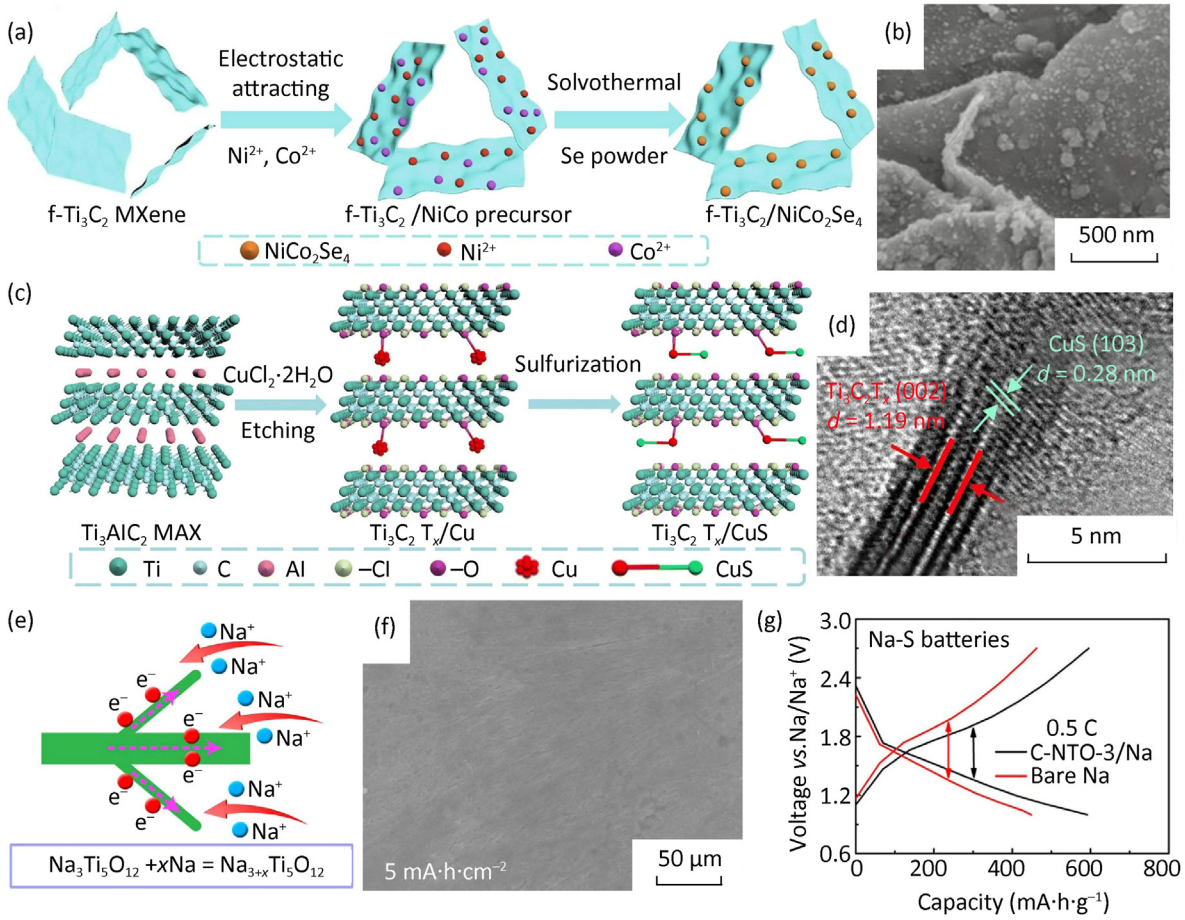

Fig. 6. (a) Schematic of the heterostructure f-Ti_3C_2/$NiCo_2Se_4$ material synthesis. (b) SEM image of f-Ti_3C_2/$NiCo_2Se_4$ flakes. Reproduced with permission [61]. Copyright 2021, Elsevier B.V. (c) Schematic of the synthesis of $Ti_3C_2T_x$/CuS heterostructure composite. (d) HRTEM images of $Ti_3C_2T_x$/CuS. Reproduced with permission [84]. Copyright 2022, The Royal Society of Chemistry. (e) Schematic and the chemical reaction equation of the reduction reaction between Na and C-NTO-3 matrix. (f) SEM image of C-NTO-3 scaffold after Na plating 5 mA·h/cm^2. (g) Charge/discharge curves of the RT Na–S batteries with C-NTO-3/Na anode and bare Na anode at 0.5C. Reproduced with permission [62]. Copyright 2020, American Chemical Society.

introduced a defect-rich and nitrogen-containing MXene named DN-MXene into the carbon nanotube (CNT) framework to form a host for the K metal anode (Fig. 7a) [58]. CNTs as the pillar supported the stable and large interlayer space between the MXene layers, which provided a porous structure to accommodate K metal and provided rapid pathways for K-ion transport (Fig. 7b). The DN-MXene alleviated the volume expansion of the anode and presented good potassium-philic characteristic due to its defects, nitrogen-containing species, and surface functional groups (−OH, −O, and −F), which delivered a low nucleation over potential of around 6 mV and guided homogeneous K metal nucleation into the porous matrix. Thereby, comparing with the traditional Cu current collectors, the DN-MXene/CNT matrix effectively prevented the direct plating of K metal outside the frameworks and significantly reduced the local current density, thus prohibiting K dendrite growth. Consequently, the K–S battery with the K@DN-MXene/CNT anode offered a high initial capacity of 638 mA·h/g and remained around 230 mA·h/g after 500 cycles at a current density of 0.5 C. Fang et al. coated the MXene ($Ti_3C_2T_x$) nanosheets onto the carbon cloth (CC) to form a $Ti_3C_2T_x$-CC host for Na metal anode (Fig. 7c–d) [59]. Due to the sodium-philic surface with high conductivity and small interface resistance derived by the MXene coating layer, the Na@$Ti_3C_2T_x$-CC anode provided a stable cycling performance and high reversible capacity in both ether-based and carbonate-based electrolytes without obvious Na dendrite growth.

Owing to the good mechanical properties, MXene nanosheets cooperate with carbon-based materials and can be exploited to prepare free-standing and flexible electrodes for Na/K-ion anode. For instance, Sun *et al.* fabricated binder and current collector free MXene/hard carbon (HC) anodes by vacuum-assisted filtration of an aqueous suspension containing HC and $Ti_3C_2T_x$ [87]. The as-prepared free-standing anode contained a 3D microporous structure, where the HC particles prevented the restacking of MXenes, by acting as spacers. Additionally, the MXene layers reduced the volume expansion of HC particles during alkali ion intercalation. A series of films with three different ratios of HC and MXene were assembled as anodes, of which the HC:MX-2:1 film achieved some of the highest reported capacities among carbon and carbide-based anodes in Na/K-ion batteries. The HC:MX-2:1 film achieved a reversible capacity of 272.3 mA·h/g after 1,500 cycles at a current density of 200 mA/g without obvious capacity loss in Na-ion batteries. In addition, HC-MX-2:1 delivered a capacity of 210 mA·h/g at 50 mA/g after 100 cycles with a capacity retention of 84% in K-ion batteries.

Except the application on anode side, the MXene/carbon-based composite is also widely used in the cathode side of the beyond-lithium batteries. MXene nanosheets can combine with carbon-based materials such as CNT microspheres [86], ultra-microporous carbon (UMC) [88], reduced graphene oxide (RGO) [63], and covalent organic framework (COF) [89]. This can optimize the microstructure of MXenes, which significantly promote the electrochemical performance of the sulfur cathode in room temperature alkali-sulfur batteries. Recently, our group reported a porous nitrogen-doped $Ti_3C_2T_x$ MXene combined with multiwalled carbon nanotube microspheres (N-MXene@MWCNT-MP) for sulfur cathodes (Fig. 7e) [86]. This MXene/carbon-based composite provided a more regular and stable morphology during cycling and thus offered a higher sulfur loading of up to 5.5 mg/cm^2. Due to the excellent elastic properties of the as-prepared composite, the spherical structure of the N-MXene@MWCNT-MP cathodes could maintain a high reversible capacity of 450.1 mA·h/g after 1,000 cycles at 2 C.

MXene/carbon-based composites have also been used to modify separators and construct functional interlayers to tackle the shuttle effect and dendrite growth in beyond-lithium metal-S/Se batteries. Zhang *et al.* firstly reported a composite separator with the CTAB modified CNT and $Ti_3C_2T_x$ MXene co-assembling on the PP separator (denoted as CCNT/MXene/PP separator) for the Na/Li–Se batteries [60]. The CNT network within the modified separator can avoid the restacking of the MXene layers and provide a wide-open channel for rapid transfer of Na ions. Additionally, the surface functional groups (−OH and −F) of MXene and the CTA^+ in CTAB can confine the soluble polyselenide species through the chemical absorption, which effectively prevent the shuttle effect and protect the metal anode from corrosion. Furthermore, due to the good mechanical property of MXene, the CCNT/MXene/PP separator displayed excellent flexibility (after being bent and folded, it returned to its original shape), which benefits the safety and cycling life of the battery. Thereby, the Na–Se battery with CCNT/MXene/PP separator delivered a good cycling performance with a high reversible capacity of 450 mA·h/g after 300 cycles at a current density of 0.5 C.

Overall, the combination of MXene and conventional carbon-based electrodes can exhibit advantages from both MXenes and the carbon-based materials. The introduction of MXenes provide various catalytic functions and specific improvement for the carbon-based materials, and the carbon-base components effectively enhance the large ion diffusion and conductivity inside the MXene nanosheets. The MXene/carbon-based composites offer a very important path to further increase the performance of the electrodes in the batteries beyond lithium without abandoning the conventional electrode materials which already have mature manufacturing procedures and production capitals.

6.4.2. MXene with polymer materials

MXene/polymer composites are mainly applied in alkali metal-S/Se batteries as the functional interlayer membranes. With the combination of the MXene with high conductivity and the polymer materials that increase the wettability and confinement capacity to the soluble polysulfides, MXene/polymer composites exhibit excellent performance to enhance the battery system. For instance, Li et al. combined the guanidinium-based iCON with Ti_3C_2 MXene (Ti_3C_2@iCON) to form an interlayer on the polypropylene (PP) separator. The iCON with high porosity and electrostatic effects attracts the soluble polysulfide species adsorption and facilitates ion transportation, and the MXene with high electronic conductivity and catalytic effects accelerated the conversion of the intermediate species, and thus effectively prohibited the shuttle effect [90]. The MXene materials can also achieve synergistic effects when coupling with other different types of functional separators such as the eggshell membrane [91], and poly(1-[3-(methacryloyloxy) propylsulfonyl]-1-(trifluoromethanesulfonyl) imide sodium) (PMTFSINa)-grafted separator [92]. Zhou *et al.* coated the defect-rich and nitrogen-containing MXene (DN-MXene) onto the cathode side of a PMTFSINa-grafted separator (which is formed by modifying the PP separator through the ultraviolet-induced surface polymerization) and obtained a PMTFSINa-grafted | DN-MXene-coated Janus separator (Fig. 8a). The DN-MXene coating layer provided a very strong polysulfides confinement and accelerated the kinetic conversion of Na polysulfides, which effectively minimized the shuttle effect. This improvement stabilized the Na metal anode, and the DN-MXene layer also significantly reduced the unnecessary porosity of the separator, preventing the dendritic Na from the metal anode to pierce through the separator, which will incur short circuits and thermal runaway. Consequently, the room temperature Na–S battery with PMTFSINa-grafted | DN-MXene-coated Janus separator, Na foil anode, and S@biomass porous carbon cathode delivered a good cycling performance with a high reversible capacity of 962 mA·h/g after 200 cycles at 0.1 C.

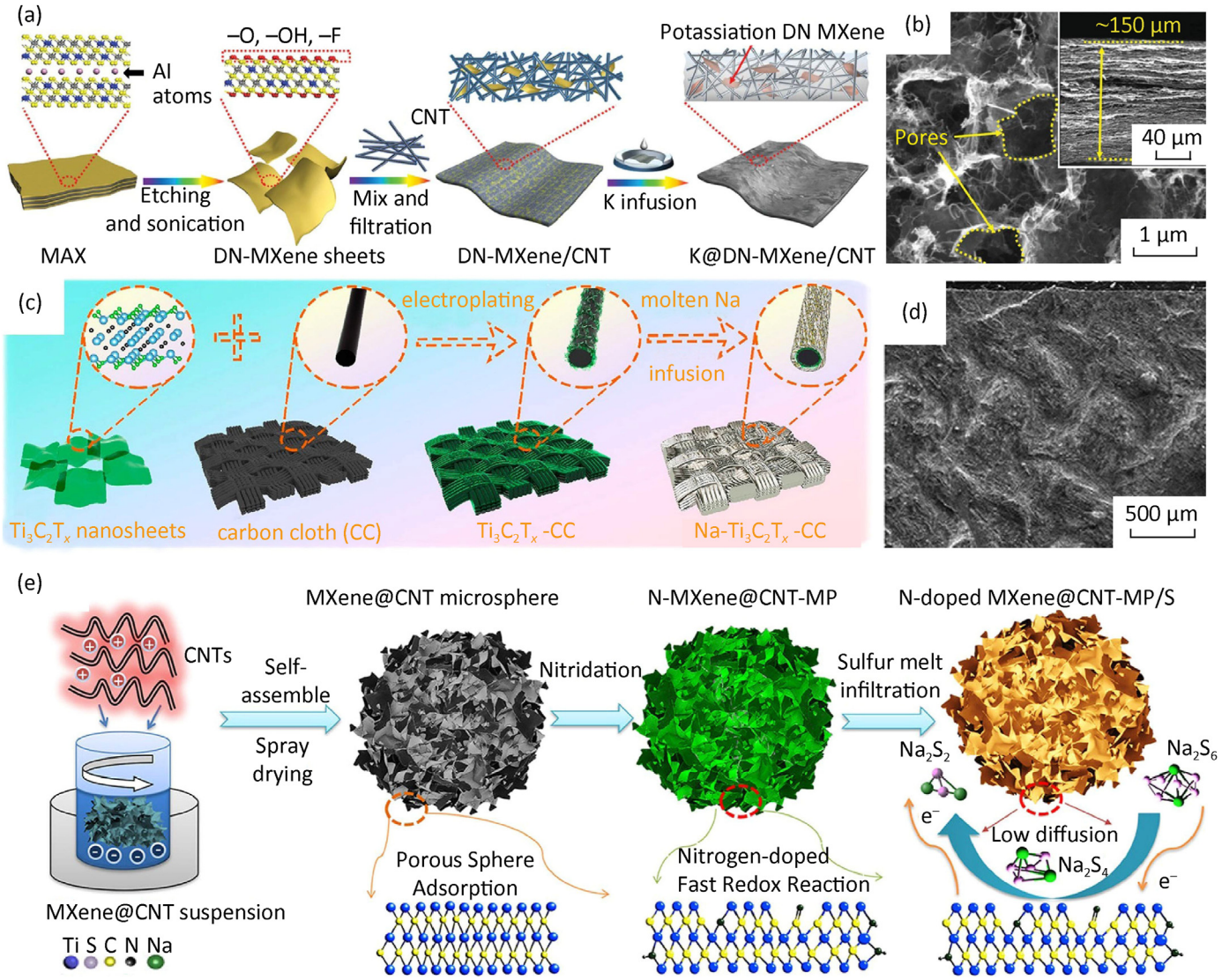

Fig. 7. (a) Schematic of the synthesis process of the DN-Mxene/CNT framework for K metal anode. (b) SEM image of the DN-Mxene/CNT framework: top view and cross-section (inset). Reproduced with permission [58]. Copyright 2019, WILEY-VCH. (c) Schematic of Na metal coated $Ti_3C_2T_x$ Mxene-carbon cloth ($Ti_3C_2T_x$-CC) matrix. (d) The SEM image of Na metal deposited $Ti_3C_2T_x$-CC scaffold with an areal capacity of ~31 mA·h/cm^2. Reproduced with permission [59]. Copyright 2020, American Chemical Society. (e) Schematic of the synthesis process of nitrogen-doped $Ti_3C_2T_x$ MXene (n-MXene) and multiwalled carbon nanotube (MWCNT) microspheres (n-MXene@MWCNT-MP) nanocomposites. Reproduced with permission [86]. Copyright 2021, American Chemical Society.

6.4.3. *MXene with alloying materials*

Alloy-based materials show prospects for large-size alkali ion storage due to their high theoretical capacity and the abundance of raw materials. However, these candidates suffer from extensive volume change during discharge and charge processes, pulverizing the electrode and deteriorating the cycling performance. For example, phosphorus (P) has the highest theoretical capacity of 2,596 mA·h/g for sodium storage based on the conversion reaction to form Na_3P alloy and a relatively low sodiation potential *vs.* Na/Na^+ [50]. Hence, combining phosphorous with conductive MXenes to fabricate nanocomposites is a promising strategy to address the individual issues and synergize their advances.

Black phosphorous (BP) is one of the most stable allotropes of phosphorus, and its layered structure lends well to exfoliation to 2D phosphorene. Guo *et al.* assembled phosphorene with $Ti_3C_2T_x$ MXene to form the phosphorene/MXene composite [50]. The hybrid material with F-rich functional groups on the surface of MXene layers facilitated the formation of a stable fluorinated SEI, allowing enhanced Coulombic efficiency. The BP layers provided increased Na storage sites and improved electronic conductivity. Furthermore, the MXene layers in the matrix improved Na-ion diffusion rate and alleviated anode structural expansion caused by the sodiation of phosphorene. Thus, the as-prepared composite anode material combined the advantages of both MXene and phosphorene, delivering a high reversible capacity and superior long cycling life (*e.g.*, around 343 mA·h/g at a current density of 1 A/g after 1,000 cycles).

More recently, Guo *et al.* designed and synthesized antimony (Sb) single atoms (SAs) and quantum dots (QDs) co-decorated 3D MXene aerogel for high-performance potassium storage (Fig. 8b–d) [93]. The Sb QDs act as potassium reservoirs relying on the alloying reaction, while the presence of Sb SAs boosts the charge transfer between Sb QDs and the MXene substrate, which contributes to the interfacial charge storage performance. Additionally, the 3D MXene aerogel provides fast electron and ion transport pathways and reinforces the structural stability of the composite electrode

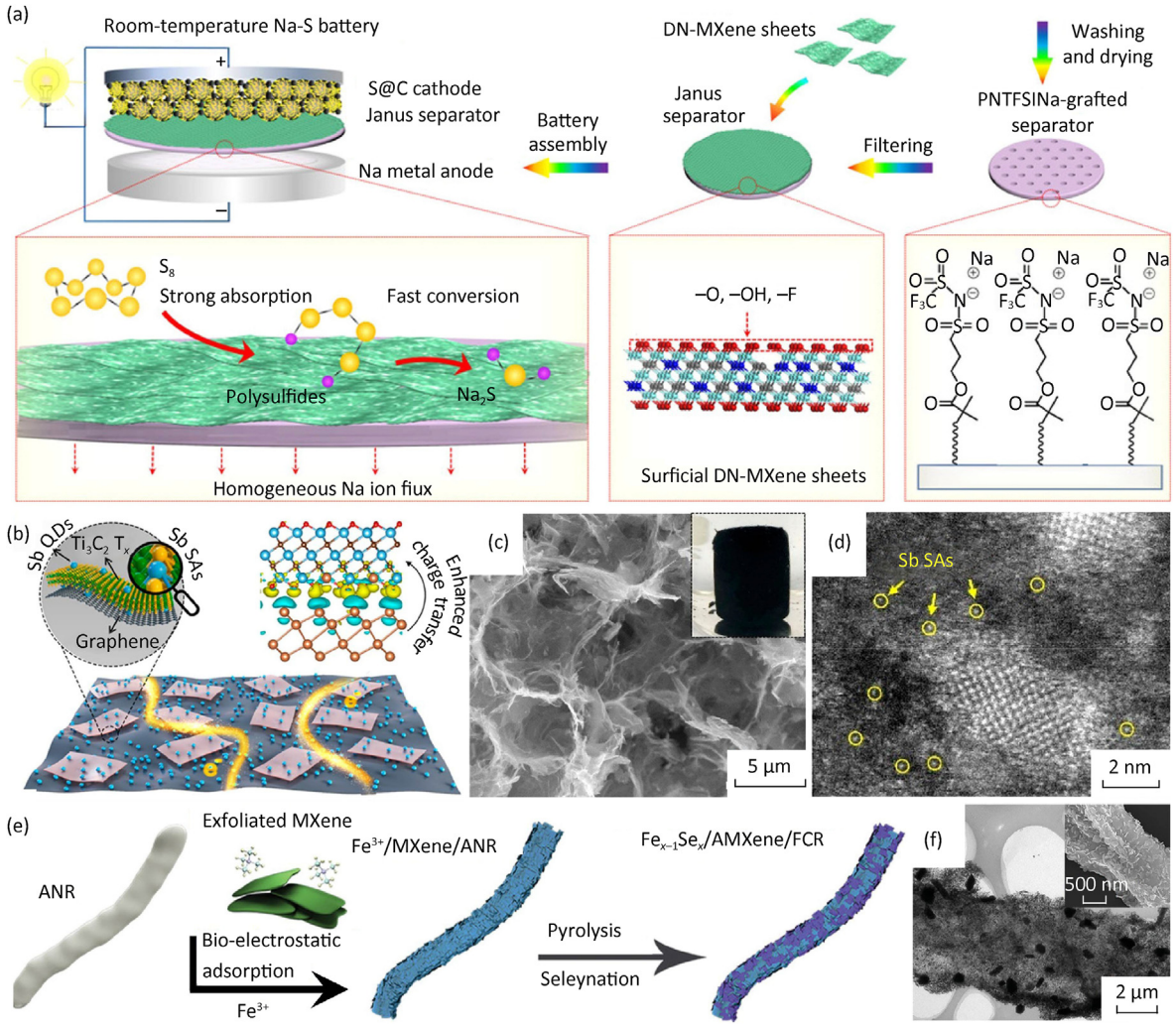

Fig. 8. (a) Schematic of the synthesis of PMTFSINa-grafted | DN-MXene-coated Janus separators using in RT Na–S batteries (Where the light cyan ball is Ti, the grey ball is C, the white ball is H, the red ball is O, the blue ball is N, the yellow ball is S, and the violet ball is Na). Reproduced with permission [92]. Copyright 2020, Wiley-VCH. (b) Schematic of the Sb SQ@MA composite. Where the light brown ball represents the Sb, blue ball represents Ti, deep brown ball represents C, and red ball represents O. (c) SEM image of the Sb SQ@MA composite (inset: the digital photo of the Sb SQ@MA composite), where SQ: antimony single atoms and quantum dots, MA: $Ti_3C_2T_x$ MXene-based aerogel. (d) HAADF (high-angle annular dark-field) image of the Sb SQ@MA composite. Reproduced with permission [93]. Copyright 2022, American Chemical Society. (e) Schematic of the $Fe_{x-1}Se_x$/MXene/FCR synthesis. (f) TEM images of $Fe_{x-1}Se_x$/MXene/FCR. Reproduced with permission [94].Copyright 2021, Wiley-VCH.

materials. Consequently, the hybrid electrode achieved an excellent rate capability and cycling performance with a capacity of 314 mA·h/g after 1,000 cycles at 1 A/g. A 2D Bismuth/MXene (Bi/Ti_3C_2) composite was reported by Ma et al. as an anode material for Na-ion batteries [95]. Through a relatively facile synthesis method, the Bi nanoparticles were evenly anchored onto the surface of the MXene nanosheets due to the adsorption of the −OH and −F surface terminals. The as-prepared materials were tested in full cells and exhibited superior specific capacity, high-rate capability, and good cycling stability. Bi/MXene anode could be stably cycled up to 2,500 times at the high current density of 5 A/g and retained a remarkable capacity of 301 mA·h/g.

6.4.4. MXene with metal chalcogenides

Metal chalcogenides are considered as promising anode candidates for rechargeable batteries due to their versatile species, natural abundance and high theoretical capacity [96]. However, the inadequate electronic conductivities and large volume expansion caused by the conversion reactions result in sluggish reaction kinetics and quick performance deterioration, rendering them unsuitable as anodes for rechargeable batteries. Recently, several researchers have attempted to synthesize the MXene-based composites by combining the layered metal oxides with MXenes to integrate their advantages and overcome the shortcomings.

For example, Guo *et al.* confined Sb_2O_3 nanoparticles in a 3D network of $Ti_3C_2T_x$ flakes through an easy solution-phase method [97]. The unique hierarchical architecture of the metal oxides/$Ti_3C_2T_x$ composite consists of a 3D network of laterally extending MXene sheets, which sandwich uniformly dispersed oxides nanomaterials, thus enhancing Na^+ diffusivity and electronic conductivity and presenting a stable and attenuated volume change of electrodes during sodiation and de-sodiation processes. Wu *et al.* synthesized a hierarchical $MoS_2/Ti_3C_2T_x$ composite with MoS_2 nanosheets evenly sandwiched between MXene nanosheets. The hybrid structure overcome the restack tendency of MoS_2 nanosheets during the fabrication, and thereby offering more efficient electrolyte percolation and ion diffusion pathways [98]. The composite material achieved a high reversible capacity of 250.9 mA·h/g at 100 mA/g and a capacity retention of 88% after 100 cycles in Na-ion batteries. Moreover, Cao et al. synthesized SnS_2 nanosheets and anchored them onto sulfur and nitrogen co-doped MXenes to create 2D SnS_2/MXene composite [99]. The obtained composite

materials were tested as the anode materials in K-ion batteries, achieving excellent reversible capacities (*e.g.*, 342.4 mA·h/g at 50 mA/g) and extremely stable cycling performance (*e.g.*, 206.1 mA·h/g at 0.5 A/g after 800 cycles).

Furthermore, MXene can also form a composite with carbonaceous materials and metal chalcogenides to improve the electrochemical performance. Cao *et al.* fabricated a composite anode material with fully exposed $Fe_{x-1}Se_x$ ($x = 2$ or 3) heterostructures, which offer a large number of electrochemically active sites [94]. This allows the formation of stable SEI and improve the efficiency of electrochemical reactions and contributed strong pseudocapacitive effects (Fig. 8e–f). The natural fungus (*i.e.*, aspergillus niger) acts as a natural bionic 1D nano-skeleton and carbon/nitrogen source, thus facilitating high electronic conductivity. The MXene nanosheet-wrapped fungal carbonaceous nanoribbons (FCR) provides conductive supporting layers for the $Fe_{x-1}Se_x$. They were subsequently tested in half cells and full cells using $Fe_{x-1}Se_x$/MXene/FCR anodes and NVP/KVP cathodes. The anode retained a reversible capacity of 348.1 mA·h/g after 2,000 cycles at a current density of 10 A/g in Na-ion batteries. Meanwhile, its K^+ storage capacity after 80 cycles was equal to 449.3 mA·h/g at 0.1 A/g with very low-capacity fade.

7. Conclusion and perspective

In conclusion, MXenes show a promising future to be applied in sustainable rechargeable batteries. Incorporating advanced surface and structure engineering, MXenes and MXene-based materials can have vast potential to boost the electrochemical performance of the rechargeable batteries beyond lithium.

MXenes are suitable electrode materials for alkali-based batteries beyond lithium due to their unique 2D crystal structure, good elasticity, various functional groups, high electronic and ionic conductivity, and excellent pseudocapacitance contribution. With the development of improvement strategies, including surface termination modification, heteroatom doping, surface coating, interlayer space expansion, nanostructure construction, heterostructures engineering and secondary material cooperation, the large-size alkali ion storage capability of MXene-based materials can be significantly enhanced.

However, the development of MXene-based materials for rechargeable batteries beyond lithium is still at the early stage, many challenges need to be overcome ahead of their practical applications. Herein, we summarize some major hurdles impeding their wide usage in batteries and offer research suggestions accordingly (Fig. 9).

(1) Exploring new MXenes and identifying their roles. Many pristine MXenes with multilayer transition metal backbones cannot fulfil the request for high-capacity electrodes because of the high molar mass and limited active sites only dispersed on the surface. Therefore, incorporating MXenes will probably reduce the energy density of rechargeable batteries compared to using carbon-based electrodes. Exploring and synthesizing new functional MXenes with M_2XT_x formula and employing them as additives rather than active materials can minimize this negative impact while utilizing the advances of MXenes.

(2) Reducing the cost of production. The MXenes are mainly produced by top-down synthesis using the HF, HF-containing solution or Lewis acids to etch the MAX materials currently. The safety control for the employment of hazardous chemicals dramatically increases the production cost and restricts the large-scale synthesis of MXenes. Further modifying the preparation route or developing a bottom-up synthesis method could be the way to realize the large-scale production of MXenes for rechargeable batteries.

(3) Improving the stability of MXene-based materials. Currently, the MXenes have poor air stability due to the easy oxidation character in the humid environment. The extra humidity control or protection protocol used in the laboratory is costly and difficult to be transferred to large-scale production. Additional antioxidation treatments or facile storage conditions need to be explored to avoid the degradation of MXenes during manufacturing. For example, surface terminations engineering by designing pure –O surface functional groups or coating MXene with air-stable metal/non-metal layers can be the research directions to enhance MXene stability.

(4) Tailoring the functionalities and expanding roles of MXenes in rechargeable batteries beyond lithium. The diverse compositions and tunable surface chemistries enable a variety of possible chemical and physical properties of MXenes. Whereas, most of the efforts have been dedicated to developing MXene-based electrode materials now. The possibilities of MXenes in beyond lithium batteries as separator modifiers, current collectors, electrolyte additives or stable interface inducers necessitate more investigations.

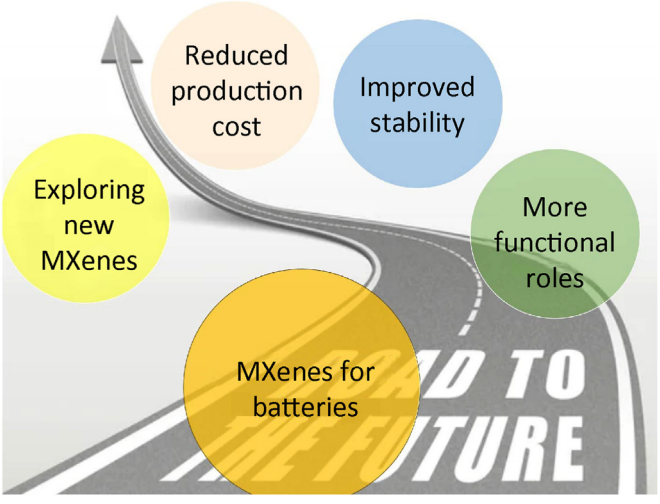

Fig. 9. Schematic of prospective research directions in developing MXene materials for rechargeable batteries beyond lithium in the future.

Declaration of competing interest

The authors declare that they have no known competing financial interests or personal relationships that could have appeared to influence the work reported in this paper.

Acknowledgement

The authors would like to thank the financial support by the Australian Research Council (ARC) through the ARC Discovery Projects (DP210101389 and DP230101579) and the ARC Research Hub for Integrated Energy Storage Solutions (IH180100020).

References

[1] Miller JR, Simon P. Electrochemical capacitors for energy management. Science 2008;321:651–2.
[2] Risacher F, Fritz B. Origin of salts and brine evolution of bolivian and chilean salars. Aquat Geochem 2009;15:123–57.
[3] Liu Y, Li J, Shen Q, Zhang J, He P, Qu X, et al. Advanced characterizations and measurements for sodium-ion batteries with nasicon-type cathode materials.

eScience 2022;2:10–31.
[4] Eames C, Islam MS. Ion intercalation into two-dimensional transition-metal carbides: global screening for new high-capacity battery materials. J Am Chem Soc 2014;136:16270–6.
[5] Er D, Li J, Naguib M, Gogotsi Y, Shenoy VB. Ti_3C_2 MXene as a high capacity electrode material for metal (Li, Na, K, Ca) ion batteries. ACS Appl Mater Interfaces 2014;6:11173–9.
[6] Moreau P, Guyomard D, Gaubicher J, Boucher F. Structure and stability of sodium intercalated phases in olivine $FePO_4$. Chem Mater 2010;22:4126–8.
[7] Lu Y, Wang L, Cheng J, Goodenough JB. Prussian blue: a new framework of electrode materials for sodium batteries. Chem Commun 2012;48:6544–6.
[8] Palomares V, Casas-Cabanas M, Castillo-Martínez E, Han MH, Rojo T. Update on Na-based battery materials. A growing research path. Energy Environ Sci 2013;6:2312–37.
[9] Singh N, Arthur TS, Ling C, Matsui M, Mizuno F. A high energy-density tin anode for rechargeable magnesium-ion batteries. Chem Commun 2013;49:149–51.
[10] Qian J, Xiong Y, Cao Y, Ai X, Yang H. Synergistic Na-storage reactions in Sn_4P_3 as a high-capacity, cycle-stable anode of Na-ion batteries. Nano Lett 2014;14:1865–9.
[11] Zhu Y, Han X, Xu Y, Liu Y, Zheng S, Xu K, et al. Electrospun Sb/C fibers for a stable and fast sodium-ion battery anode. ACS Nano 2013;7:6378–86.
[12] Darwiche A, Marino C, Sougrati MT, Fraisse B, Stievano L, Monconduit L. Better cycling performances of bulk Sb in Na-ion batteries compared to Li-ion systems: an unexpected electrochemical mechanism. J Am Chem Soc 2012;134:20805–11.
[13] Tang K, Fu L, White RJ, Yu L, Titirici M-M, Antonietti M, et al. Hollow carbon nanospheres with superior rate capability for sodium-based batteries. Adv Energy Mater 2012;2:873–7.
[14] Yang J, Wang T, Guo X, Sheng X, Li J, Wang C, et al. Flexible sodium-ion capacitors boosted by high electrochemically-reactive and structurally-stable Sb_2S_3 nanowire/$Ti_3C_2T_x$ mxene film anodes. Nano Res 2023;16:5592–600.
[15] Wang S, Zhao S, Guo X, Wang G. 2D material-based heterostructures for rechargeable batteries. Adv Energy Mater 2022;12:2100864.
[16] VahidMohammadi A, Rosen J, Gogotsi Y. The world of two-dimensional carbides and nitrides (MXenes). Science 2021;372:eabf1581.
[17] Naguib M, Kurtoglu M, Presser V, Lu J, Niu J, Heon M, et al. Two-dimensional nanocrystals produced by exfoliation of Ti_3AlC_2. Adv Mater 2011;23:4248–53.
[18] Naguib M, Mashtalir O, Carle J, Presser V, Lu J, Hultman L, et al. Two-dimensional transition metal carbides. ACS Nano 2012;6:1322–31.
[19] Naguib M, Mochalin VN, Barsoum MW, Gogotsi Y. 25th anniversary article: MXenes: a new family of two-dimensional materials. Adv Mater 2014;26:992–1005.
[20] Wang X, Kajiyama S, Iinuma H, Hosono E, Oro S, Moriguchi I, et al. Pseudocapacitance of MXene nanosheets for high-power sodium-ion hybrid capacitors. Nat Commun 2015;6:6544.
[21] Ghidiu M, Naguib M, Shi C, Mashtalir O, Pan LM, Zhang B, et al. Synthesis and characterization of two-dimensional Nb_4C_3 (MXene). Chem Commun 2014;50:9517–20.
[22] Zhao M-Q, Xie X, Ren CE, Makaryan T, Anasori B, Wang G, et al. Hollow MXene spheres and 3D macroporous MXene frameworks for Na-ion storage. Adv Mater 2017;29:1702410.
[23] Zhang C, Anasori B, Seral-Ascaso A, Park S-H, McEvoy N, Shmeliov A, et al. Transparent, flexible, and conductive 2D titanium carbide (MXene) films with high volumetric capacitance. Adv Mater 2017;29:1702678.
[24] Aslam MK, Xu M. A mini-review: Mxene composites for sodium/potassium-ion batteries. Nanoscale 2020;12:15993–6007.
[25] Aslam MK, Niu Y, Xu M. MXenes for non-lithium-ion (Na, K, Ca, Mg, and Al) batteries and supercapacitors. Adv Energy Mater 2021;11:2000681.
[26] Ming F, Liang H, Huang G, Bayhan Z, Alshareef HN. Mxenes for rechargeable batteries beyond the lithium-ion. Adv Mater 2021;33:2004039.
[27] Bhat A, Anwer S, Bhat KS, Mohideen MIH, Liao K, Qurashi A. Prospects challenges and stability of 2D MXenes for clean energy conversion and storage applications. npj 2D Mater Appl 2021;5:61.
[28] Li J, Guo C, Li CM. Recent advances of two-dimensional (2D) MXenes and phosphorene for high-performance rechargeable batteries. ChemSusChem 2020;13:1047–70.
[29] Gogotsi Y, Anasori B. The rise of MXenes. ACS Nano 2019;13:8491–4.
[30] Zhao C, Wang Q, Yao Z, Wang J, Sánchez-Lengeling B, Ding F, et al. Rational design of layered oxide materials for sodium-ion batteries. Science 2020;370:708–11.
[31] Anasori B, Lukatskaya MR, Gogotsi Y. 2D metal carbides and nitrides (MXenes) for energy storage. Nat Rev Mater 2017;2:16098.
[32] Anasori B, Gogotsi Y. 2D metal carbides and nitrides (MXenes): structure, properties and applications. Introduction to 2D transition metal carbides and nitrides (MXenes). Cham: Springer International Publishing; 2019. p. 3–12.
[33] Hong W, Wyatt BC, Nemani SK, Anasori B. Double transition-metal MXenes: atomistic design of two-dimensional carbides and nitrides. MRS Bull 2020;45:850–61.
[34] Xu X, Yang L, Zheng W, Zhang H, Wu F, Tian Z, et al. MXenes with applications in supercapacitors and secondary batteries: a comprehensive review. Mater Rep Energy 2022;2:100080.
[35] Ronchi RM, Arantes JT, Santos SF. Synthesis, structure, properties and applications of mxenes: current status and perspectives. Ceram Int 2019;45:18167–88.
[36] Zhang T, Zhang L, Hou Y. MXenes: synthesis strategies and lithium-sulfur battery applications. eScience 2022;2:164–82.
[37] Lei Y-J, Yan Z-C, Lai W-H, Chou S-L, Wang Y-X, Liu H-K, et al. Tailoring MXene-based materials for sodium-ion storage: synthesis, mechanisms, and applications. Electrochem Energy Rev 2020;3:766–92.
[38] Zhang C, Ma Y, Zhang X, Abdolhosseinzadeh S, Sheng H, Lan W, et al. Two-dimensional transition metal carbides and nitrides (MXenes): synthesis, properties, and electrochemical energy storage applications. Energy Environ Mater 2020;3:29–55.
[39] Liu A, Liang X, Ren X, Guan W, Ma T. Recent progress in MXene-based materials for metal-sulfur and metal-air batteries: potential high-performance electrodes. Electrochem Energy Rev 2022;5:112–44.
[40] An Y, Tian Y, Man Q, Shen H, Liu C, Xiong S, et al. Fluorine- and acid-free strategy toward scalable fabrication of two-dimensional mxenes for sodium-ion batteries. Nano Lett 2023;23:5217–26.
[41] Wang F, Jin S, Du Y, Xia Q, Wang L, Zhou A. Preparation of Mo_2CT_x MXene as co-catalyst for H_2 production by etching of pure/mixed HBr solution. Diamond Relat Mater 2023;136:109922.
[42] Lukatskaya MR, Mashtalir O, Ren CE, Dall'Agnese Y, Rozier P, Taberna PL, et al. Cation intercalation and high volumetric capacitance of two-dimensional titanium carbide. Science 2013;341:1502–5.
[43] Xie Y, Dall'Agnese Y, Naguib M, Gogotsi Y, Barsoum MW, Zhuang HL, et al. Prediction and characterization of MXene nanosheet anodes for non-lithium-ion batteries. ACS Nano 2014;8:9606–15.
[44] Kajiyama S, Szabova L, Sodeyama K, Iinuma H, Morita R, Gotoh K, et al. Sodium-ion intercalation mechanism in MXene nanosheets. ACS Nano 2016;10:3334–41.
[45] Bak S-M, Qiao R, Yang W, Lee S, Yu X, Anasori B, et al. Na-ion intercalation and charge storage mechanism in 2D vanadium carbide. Adv Energy Mater 2017;7:1700959.
[46] Wang X, Shen X, Gao Y, Wang Z, Yu R, Chen L. Atomic-scale recognition of surface structure and intercalation mechanism of Ti_3C_2X. J Am Chem Soc 2015;137:2715–21.
[47] Yu T, Zhao Z, Liu L, Zhang S, Xu H, Yang G. TiC_3 monolayer with high specific capacity for sodium-ion batteries. J Am Chem Soc 2018;140:5962–8.
[48] Naguib M, Adams RA, Zhao Y, Zemlyanov D, Varma A, Nanda J, et al. Electrochemical performance of MXenes as K-ion battery anodes. Chem Commun 2017;53:6883–6.
[49] Fan K, Ying Y, Li X, Luo X, Huang H. Theoretical investigation of V_3C_2 MXene as prospective high-capacity anode material for metal-ion (Li, Na, K, and Ca) batteries. J Phys Chem C 2019;123:18207–14.
[50] Guo X, Zhang W, Zhang J, Zhou D, Tang X, Xu X, et al. Boosting sodium storage in two-dimensional phosphorene/$Ti_3C_2T_x$ MXene nanoarchitectures with stable fluorinated interphase. ACS Nano 2020;14:3651–9.
[51] Zhao Y, Zhang J, Guo X, Cao X, Wang S, Liu H, et al. Engineering strategies and active site identification of MXene-based catalysts for electrochemical conversion reactions. Chem Soc Rev 2023;52:3215–64.
[52] Kamysbayev V, Filatov AS, Hu H, Rui X, Lagunas F, Wang D, et al. Covalent surface modifications and superconductivity of two-dimensional metal carbide MXenes. Science 2020;369:979–83.
[53] Bao W, Shuck CE, Zhang W, Guo X, Gogotsi Y, Wang G. Boosting performance of Na–S batteries using sulfur-doped $Ti_3C_2T_x$ MXene nanosheets with a strong affinity to sodium polysulfides. ACS Nano 2019;13:11500–9.
[54] Huang H, Cui J, Liu G, Bi R, Zhang L. Carbon-coated $MoSe_2$/MXene hybrid nanosheets for superior potassium storage. ACS Nano 2019;13:3448–56.
[55] Luo J, Wang C, Wang H, Hu X, Matios E, Lu X, et al. Pillared MXene with ultralarge interlayer spacing as a stable matrix for high performance sodium metal anodes. Adv Funct Mater 2019;29:1805946.
[56] Luo J, Zhang W, Yuan H, Jin C, Zhang L, Huang H, et al. Pillared structure design of MXene with ultralarge interlayer spacing for high-performance lithium-ion capacitors. ACS Nano 2017;11:2459–69.
[57] Li J, Yan D, Hou S, Li Y, Lu T, Yao Y, et al. Improved sodium-ion storage performance of $Ti_3C_2T_x$ MXenes by sulfur doping. J Mater Chem A 2018;6:1234–43.
[58] Tang X, Zhou D, Li P, Guo X, Sun B, Liu H, et al. MXene-based dendrite-free potassium metal batteries. Adv Mater 2020;32:1906739.
[59] Fang Y, Lian R, Li H, Zhang Y, Gong Z, Zhu K, et al. Induction of planar sodium growth on mxene ($Ti_3C_2T_x$)-modified carbon cloth hosts for flexible sodium metal anodes. ACS Nano 2020;14:8744–53.
[60] Zhang F, Guo X, Xiong P, Zhang J, Song J, Yan K, et al. Interface engineering of MXene composite separator for high-performance Li–Se and Na–Se batteries. Adv Energy Mater 2020;10:2000446.
[61] Huang P, Zhang S, Ying H, Zhang Z, Han W. Few-layered Ti_3C_2 MXene anchoring bimetallic selenide $NiCo_2Se_4$ nanoparticles for superior sodium-ion batteries. Chem Eng J 2021;417:129161.
[62] Luo J, Lu X, Matios E, Wang C, Wang H, Zhang Y, et al. Tunable MXene-derived 1D/2D hybrid nanoarchitectures as a stable matrix for dendrite-free and ultrahigh capacity sodium metal anode. Nano Lett 2020;20:7700–8.
[63] Yang Q, Yang T, Gao W, Qi Y, Guo B, Zhong W, et al. An MXene-based aerogel with cobalt nanoparticles as an efficient sulfur host for room-temperature Na–S batteries. Inorg Chem Front 2020;7:4396–403.
[64] Chen H, Zhang T, Wei C, Wang J, Niu X. First-principle study of Ti_2XS_2 (X = C/N) MXenes as high capacity anodes for rechargeable potassium-ion batteries. Appl Surf Sci 2021;546:149096.
[65] Natu V, Pai R, Sokol M, Carey M, Kalra V, Barsoum MW. 2D $Ti_3C_2T_z$ MXene

synthesized by water-free etching of Ti_3AlC_2 in polar organic solvents. Chem 2020;6:616–30.
[66] Yang C, Tang Y, Tian Y, Luo Y, Faraz Ud Din M, Yin X, et al. Flexible nitrogen-doped 2D titanium carbides (MXene) films constructed by an ex situ solvothermal method with extraordinary volumetric capacitance. Adv Energy Mater 2018;8:1802087.
[67] Zhang J, Zhao Y, Guo X, Chen C, Dong C-L, Liu R-S, et al. Single platinum atoms immobilized on an MXene as an efficient catalyst for the hydrogen evolution reaction. Nat Catal 2018;1:985–92.
[68] Zhang L, Wang Z, Chen W, Yuan R, Zhan K, Zhu M, et al. Fe_3O_4 nanoplates anchored on $Ti_3C_2T_x$ MXene with enhanced pseudocapacitive and electrocatalytic properties. Nanoscale 2021;13:15343–51.
[69] Wang Y, Gu F, Cao L, Fan L, Hou T, Zhu Q, et al. TiCN MXene hybrid BCN nanotubes with trace level Co as an efficient ORR electrocatalyst for Zn-air batteries. Int J Hydrogen Energy 2022;47:20894–904.
[70] Zhang X, Ni Z, Bai X, Shen H, Wang Z, Wei C, et al. Hierarchical porous N-doped carbon encapsulated fluorine-free MXene with tunable coordination chemistry by one-pot etching strategy for lithium–sulfur batteries. Adv Energy Mater 2023;13:2301349.
[71] Mashtalir O, Naguib M, Mochalin VN, Dall'Agnese Y, Heon M, Barsoum MW, et al. Intercalation and delamination of layered carbides and carbonitrides. Nat Commun 2013;4:1716.
[72] Ghidiu M, Halim J, Kota S, Bish D, Gogotsi Y, Barsoum MW. Ion-exchange and cation solvation reactions in Ti_3C_2 MXene. Chem Mater 2016;28:3507–14.
[73] Wu Y, Nie P, Wang J, Dou H, Zhang X. Few-layer MXenes delaminated via high-energy mechanical milling for enhanced sodium-ion batteries performance. ACS Appl Mater Interfaces 2017;9:39610–7.
[74] Luo J, Zheng J, Nai J, Jin C, Yuan H, Sheng O, et al. Atomic sulfur covalently engineered interlayers of Ti_3C_2 MXene for ultra-fast sodium-ion storage by enhanced pseudocapacitance. Adv Funct Mater 2019;29:1808107.
[75] Zhang S, Ying H, Huang P, Wang J, Zhang Z, Zhang Z, et al. Ultrafine Sb pillared few-layered $Ti_3C_2T_x$ MXenes for advanced sodium storage. ACS Appl Energy Mater 2021;4:9806–15.
[76] Zhao S, Liu Z, Xie G, Guo X, Guo Z, Song F, et al. Achieving high-performance 3D K^+-pre-intercalated $Ti_3C_2T_x$ MXene for potassium-ion hybrid capacitors via regulating electrolyte solvation structure. Angew Chem Int Ed 2021;60:26246–53.
[77] Lian P, Dong Y, Wu Z-S, Zheng S, Wang X, Sen W, et al. Alkalized Ti_3C_2 MXene nanoribbons with expanded interlayer spacing for high-capacity sodium and potassium ion batteries. Nano Energy 2017;40:1–8.
[78] Dong Y, Wu Z-S, Zheng S, Wang X, Qin J, Wang S, et al. Ti_3C_2 MXene-derived sodium/potassium titanate nanoribbons for high-performance sodium/potassium ion batteries with enhanced capacities. ACS Nano 2017;11:4792–800.
[79] Natu V, Clites M, Pomerantseva E, Barsoum MW. Mesoporous MXene powders synthesized by acid induced crumpling and their use as Na-ion battery anodes. Mater Res Lett 2018;6:230–5.
[80] Zhao D, Clites M, Ying G, Kota S, Wang J, Natu V, et al. Alkali-induced crumpling of $Ti_3C_2T_x$ (MXene) to form 3D porous networks for sodium ion storage. Chem Commun 2018;54:4533–6.
[81] Xie X, Kretschmer K, Anasori B, Sun B, Wang G, Gogotsi Y. Porous $Ti_3C_2T_x$ MXene for ultrahigh-rate sodium-ion storage with long cycle life. ACS Appl Nano Mater 2018;1:505–11.
[82] Liu Y-T, Zhang P, Sun N, Anasori B, Zhu Q-Z, Liu H, et al. Self-assembly of transition metal oxide nanostructures on MXene nanosheets for fast and stable lithium storage. Adv Mater 2018;30:1707334.
[83] Yang C, Liu Y, Sun X, Zhang Y, Hou L, Zhang Q, et al. In-situ construction of hierarchical accordion-like TiO_2/Ti_3C_2 nanohybrid as anode material for lithium and sodium ion batteries. Electrochim Acta 2018;271:165–72.
[84] Huang P, Ying H, Zhang S, Zhang Z, Han W-Q. In situ fabrication of MXene/CuS hybrids with interfacial covalent bonding via lewis acidic etching route for efficient sodium storage. J Mater Chem A 2022;10:22135–44.
[85] Zhao R, Qian Z, Liu Z, Zhao D, Hui X, Jiang G, et al. Molecular-level heterostructures assembled from layered black phosphorene and Ti_3C_2 MXene as superior anodes for high-performance sodium ion batteries. Nano Energy 2019;65:104037.
[86] Bao W, Wang R, Qian C, Zhang Z, Wu R, Zhang Y, et al. Porous heteroatom-doped $Ti_3C_2T_x$ MXene microspheres enable strong adsorption of sodium polysulfides for long-life room-temperature sodium–sulfur batteries. ACS Nano 2021;15:16207–17.
[87] Sun N, Zhu Q, Anasori B, Zhang P, Liu H, Gogotsi Y, et al. MXene-bonded flexible hard carbon film as anode for stable Na/K-ion storage. Adv Funct Mater 2019;29:1906282.
[88] Zhao Q, Zhu Q, Miao J, Zhang P, Xu B. 2D MXene nanosheets enable small-sulfur electrodes to be flexible for lithium–sulfur batteries. Nanoscale 2019;11:8442–8.
[89] Yang Z, Peng C, Meng R, Zu L, Feng Y, Chen B, et al. Hybrid anatase/rutile nanodots-embedded covalent organic frameworks with complementary polysulfide adsorption for high-performance lithium–sulfur batteries. ACS Cent Sci 2019;5:1876–83.
[90] Li P, Lv H, Li Z, Meng X, Lin Z, Wang R, et al. The electrostatic attraction and catalytic effect enabled by ionic–covalent organic nanosheets on mxene for separator modification of lithium–sulfur batteries. Adv Mater 2021;33:2007803.
[91] Yin L, Xu G, Nie P, Dou H, Zhang X. MXene debris modified eggshell membrane as separator for high-performance lithium-sulfur batteries. Chem Eng J 2018;352:695–703.
[92] Zhou D, Tang X, Guo X, Li P, Shanmukaraj D, Liu H, et al. Polyolefin-based janus separator for rechargeable sodium batteries. Angew Chem Int Ed 2020;59:16725–34.
[93] Guo X, Gao H, Wang S, Yang G, Zhang X, Zhang J, et al. MXene-based aerogel anchored with antimony single atoms and quantum dots for high-performance potassium-ion batteries. Nano Lett 2022;22:1225–32.
[94] Cao J, Wang L, Li D, Yuan Z, Xu H, Li J, et al. $Ti_3C_2T_x$ MXene conductive layers supported bio-derived $Fe_{x-1}Se_x$/MXene/carbonaceous nanoribbons for high-performance half/full sodium-ion and potassium-ion batteries. Adv Mater 2021;33:2101535.
[95] Ma H, Li J, Yang J, Wang N, Liu Z, Wang T, et al. Bismuth nanoparticles anchored on $Ti_3C_2T_x$ MXene nanosheets for high-performance sodium-ion batteries. Chem Asian J 2021;16:3774–80.
[96] Sajjad M, Cheng F, Lu W. Research progress in transition metal chalcogenide based anodes for K-ion hybrid capacitor applications: a mini-review. RSC Adv 2021;11:25450–60.
[97] Guo X, Xie X, Choi S, Zhao Y, Liu H, Wang C, et al. Sb_2O_3/MXene($Ti_3C_2T_x$) hybrid anode materials with enhanced performance for sodium-ion batteries. J Mater Chem A 2017;5:12445–52.
[98] Wu Y, Nie P, Jiang J, Ding B, Dou H, Zhang X. MoS_2-nanosheet-decorated 2D titanium carbide (MXene) as high-performance anodes for sodium-ion batteries. Chemelectrochem 2017;4:1560–5.
[99] Cao Y, Chen H, Shen Y, Chen M, Zhang Y, Zhang L, et al. SnS_2 nanosheets anchored on nitrogen and sulfur Co-doped MXene sheets for high-performance potassium-ion batteries. ACS Appl Mater Interfaces 2021;13:17668–76.

Zefu Huang was graduated from the University of Sydney and obtained a Master of Professional Engineering (Chemical and biomolecular) degree in 2019. Currently, he is a Ph.D. candidate in the Centre for Clean Energy Technology (CCET) at the University of Technology Sydney (UTS), Australia. His research interests include sodium-ion batteries, sodium–sulfur batteries, and 2D materials.

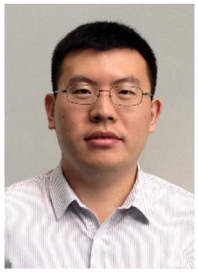

Bing Sun received his Ph.D. in 2012 at University of Technology Sydney (UTS), Australia. Currently, he is a research associate in the Centre for Clean Energy Technology at University of Technology Sydney. His research interests focus on the development of next-generation battery materials and technology for lithium-based batteries and sodium-based batteries. He is the recipient of Australian Research Council (ARC) Discovery Early Career Researcher Award (DECRA) 2018 and ARC Future Fellowship 2022.

Prof. Guoxiu Wang is the Director of the Centre for Clean Energy Technology and a Distinguished Professor at University of Technology Sydney (UTS), Australia. His research interests include lithium-ion batteries, lithium-air batteries, sodium-ion batteries, lithium-sulfur batteries, supercapacitors, hydrogen storage materials, fuel-cells, 2D materials, and electrocatalysis for hydrogen production. Professor Wang has published more than 650 refereed journal papers with an h-index of 134. His publications have attracted over 59,800 citations. He has been listed as a highly cited researcher in both Materials Science and Chemistry by Web of Science/Clarivate Analytics in 2018 and 2022 and a highly cited researcher in Materials Science in 2019, 2020 and 2021.